Catestatin (CST) is a key mediator of the immunoendocrine regulation of cardiovascular function

Wei Ying[2*], Kechun Tang[1*], Ennio Avolio[2], Jan M. Schilling[1,3*], Teresa Pasqua[2], Matthew A. Liu[2], Sumana Mahata[2], Gautam Bandyopadhyay[2], Soumita Das[4], Debashis Sahoo[5,6,] Nicholas J.G. Webster[1,3], Hemal H. Patel[1,3] Pradipta Ghosh[1,2,7] and Sushil K. Mahata[1,2¶].

[1]VA San Diego Healthcare System, 3350 La Jolla Village Drive, San Diego, CA, USA
[2]Department of Medicine, University of California San Diego, La Jolla, CA, USA,
[3]Department of Anesthesiology, University of California San Diego, La Jolla, CA, USA,
[4]Department of Pathology, University of California San Diego, La Jolla, CA, USA,
[5]Department of Pediatrics, University of California San Diego, CA, USA,
[6]Department of Computer Science and Engineering, Jacob's School of Engineering, University of California San Diego, La Jolla, USA,
[7]Department of Cellular and Molecular Medicine, University of California San Diego, La Jolla, CA, USA.

*Contributed equally to this work.

¶**Correspondence should be addressed to**: Sushil K. Mahata, Metabolic Physiology & Ultrastructural Biology Laboratory, Department of Medicine, University of California San Diego, 9500 Gilman Drive, La Jolla, CA 92093-0732, smahata@health.ucsd.edu.

Abstract

Objective: Hypertension (HTN) is a global pandemic, affecting more than one billion people. Although catestatin (CST), a chromogranin A (CgA)-derived peptide, decreases blood pressure (BP) in rodent models of HTN, the mechanisms underlying its hypotensive action is yet to be established. Here we generated CST knockout (CST-KO) mice to pinpoint the mechanism of the hypotensive action of CST.

Methods and Results: CST-KO mice were hypertensive; their serum cytokines were elevated, anti-inflammatory genes were downregulated, and their hearts showed marked infiltration with macrophages. CST replenishment reversed all these phenotypes - it normalized BP, reduced serum cytokines, upregulated anti-inflammatory genes, and reduced the cardiac infiltrates by ~30%, as determined by FACS. Pre-conditioning-induced cardioprotection was also abolished in CST-KO mice. We hypothesize that CST's anti-hypertensive and cardioprotective effects may be caused by suppressed trafficking of macrophages to the heart and reduced inflammation. Such *cause-and-effect* relationship is supported by the fact that CST-KO mice became normotensive when they were depleted of macrophages using chlodronate, or when they received bone marrow transplant from wild-type littermates. Mechanistically, cardiac tissue transcriptomes revealed multiple altered gene expression programs in CST-KO mice that are commonly encountered in human cardiomyopathies. Among others, a prominent reduction of *Glo1* gene was seen in CST-KO mice; supplementation with CST increased it expression by >7-fold. Because *Glo*1 in macrophages metabolizes methylglyoxal, an inflammatory agent whose accumulation promotes vascular damage in HTN and T2DM, this could be one of the means by which CST attenuates inflammation and improves cardiovascular health. Repletion of CST also improved glucose metabolism and increased the surface area of mitochondrial cristae and decreased the secretion of catecholamines; the latter explains the anti-hypertensive actions of CST.

Conclusions: We conclude that the anti-hypertensive effects of CST is mediated at least in part via CST's anti-inflammatory actions; in the absence of CST, macrophages are more reactive, they infiltrate the heart and alter the ultrastructure, physiologic and molecular makeup of the myocardium. These studies implicate CST as a key mediator of the observed crosstalk between systemic and cardiac inflammation in HTN.

Abbreviations

2DG: 2-deoxy-glucose
Actc1: cardiac muscle actin alpha
Atp5j: mitochondrial ATP synthase subunit F6
BRS: baroreflex sensitivity
Cd36: cluster of differentiation 36
Cers2: ceramide synthase 2
CgA: chromogranin A
CST: catestatin
CST-KO: CST knockout
DCM: diabetic cardiomyopathy
ER: endoplasmic reticulum
FA: fatty acid
FRT: Flp recognition target
G6P: glucose-6-phosphate
Glut4: glucose transporter 4
GO: gene ontology
GSK-3b: glycogen synthase kinase-3 beta
HCM: hypertrophic cardiomyopathy
HRV: heart rate variability
IFM: inter/intramyofibrillar mitochondria
IPC: ischemic preconditioning
LVDP: left ventricular developed pressure
LVEDP: left ventricular end diastolic pressure
Myl4: myosin light chain 4
Myl7: myosin light chain 7
mPTP: mitochondrial permeability transition pore
Myh7: myosin heavy chain 7
NADH: nicotinamide adenine dinucleotide hydride
NCD: normal chow diet
Pdk2: pyruvate dehydrogenase kinase 2
Pfkm: phosphofructokinase, muscle form
PI3K: phosphoinositide 3-kinase
PINK1: PTEN-induced putative kinase 1
Ppara: peroxisome proliferator-activated receptor alpha
qPCR: quantitative polymerase chain reaction
SBP: systolic blood pressure
Sdhc: succinate dehydrogenase complex subunit c
Slc27a1: solute carrier family 27 member 1
Slc27a2: solute carrier family 27 member 2
Sptlc1: serine palmitoyltransferase long-chain base subunit 1
SSM: subsarcolemmal mitochondria
T2DM: Type 2 diabetes mellitus
TCA: trichloroacetic acid
TEM: transmission electron microscopy
Tnni3: cardiac Troponin I
Tnnt2: cardiac Troponin T2
Tpm: tropomyosin
Ttn: Titin

122 **Introduction**

123

124 Hypertension (HTN) is an important risk factor for cardiovascular disease (CVD) and mortality [1].
125 The burden of HTN and the estimated HTN-associated deaths have increased substantially over
126 the past 25 years [2].

127 The role of catecholamines (CAs), e.g., dopamine (DA), norepinephrine (NE), and
128 epinephrine (Epi) in the regulation of blood pressure (BP) and their dysregulated secretion or
129 function in HTN has been well recognized [3-7]. These CAs are produced and secreted by
130 neuroendocrine cells e.g., chromaffin cells in the adrenal medulla and have dual hormone and
131 neurotransmitter functions. Once released, CAs interact with numerous adrenergic receptors in a
132 variety of tissues to impose an intricate neuro-hormonal regulation of BP.

133 Besides the CAs, the immune system is also recognized for its role in the genesis and
134 progression of HTN[8-11]. Inflammation is an essential component of many diseases, and the
135 connections between innate and adaptive immunity, HTN, and CVD add support to the role of the
136 immune system in cardiovascular pathology [11, 12]. Known as integrators of neural, hormonal, and
137 immune signals, it has been shown that inflammation influences CA biosynthesis by adrenal
138 medullary cells. The converse, i.e., how CAs may impact inflammation remains unknown. More
139 specifically, although the impact of immune activation and inflammation in the regulation of HTN
140 is evolving, the specific immunologic mechanisms that contribute to the pathogenesis of HTN are
141 incompletely understood. Here we reveal an unexpected role of how the process of CA secretion
142 and its impact on systemic HTN is fueled by an immunologic phenomenon *via* Chromogranin A
143 (CgA), and more specifically, its proteolytic biologic fragment, catestatin (CST: $hCgA_{352-372}$) [13].

144 Co-stored and co-released with Cas, CgA, a ~49 kDa secretory proprotein [14-16] is
145 overexpressed in humans with essential HTN [17, 18] and in rodent genetic models of HTN [19]. Unlike
146 CgA, plasma CST levels are diminished not only in essential HTN [18, 20] but also in the
147 normotensive offspring of patients with HTN [20]. Additionally, HTN-associated SNPs within the
148 CST segment of CgA have been extensively evaluated [21-28]. Processing of CgA to CST is low in
149 patients with HTN and heart failure [18, 29], suggesting dysregulation in the processing of CgA to
150 CST in CVD. Furthermore, both CgA heterozygote (CgA+/-) and CgA knockout (CgA-/-) mice are
151 hypertensive [30]; but treatment with CST decreases BP and the levels of plasma CAs to that seen
152 in control littermates. Although these findings, especially the repletion studies, point to the
153 importance of CST and its sufficiency in reversing HTN, none conclusively show that CST is
154 necessary. This is because CgA has many biologically active peptides, and it is possible that any
155 or many of these CgA-derived peptides could be confounding the findings in these studies.

156 To mitigate these issues, and pinpoint the actions of CST, we generated a precise tool,
157 i.e., CST-KO mice. Given the hypertensive, hyperadrenergic, and inflammatory phenotypes in
158 these mice, we used that as a model to dissect the role of CST in the maintenance of
159 cardiovascular homeostasis. Our studies revealed a complex interplay between a trifecta: the
160 innate immune system, CA secretion from chromaffin cells in the adrenal medulla, and the
161 cardiovascular system, all coordinated by CST.
162
163

164 **Material and Methods**

165

166 **Mice**. To generate CST-KO mice, we selectively targeted to eliminate the 63 bp CST encoding
167 segment from Exon VII of the *Chga* gene. The general cloning strategy involved PCR and
168 subcloning into pBluescript. We introduced a diphtheria toxin sequence to serve as a negative
169 selection at the 3'-end of the construct that would enrich (by ~5-fold) positive clones after
170 transfection of the targeted construct into ES cells by electroporation. For positive selection by
171 G418 we have introduced a Neo cassette flanked by FRT (*Flp* recognition target) site. PCR
172 screening of CST-KO mice are shown in **Fig. S1.**
173 Male WT and CST-KO (20-24 weeks old) with a mixed genetic background (50%
174 129svJ/50% C57BL/6) were studied. Mice were kept in a 12 hr dark/light cycle and fed a normal
175 chow diet (NCD: 13.5% calorie from fat; LabDiet 5001, Lab Supply, Fort Worth, TX). All studies
176 with mice were approved by the UCSD and Veteran Affairs San Diego Institutional Animal Care
177 and Use Committees (IACUC) and conform to relevant National Institutes of Health guidelines.

178

179 **Protein analysis by immunobloting.** Left ventricles were homogenized in a buffer containing
180 phosphatase and protease inhibitors, as previously described [31]. Homogenates were subjected
181 to SDS-PAGE and immunoblotted. Primary antibodies for phosphorylated and total AKT and
182 GSK-3β were from Cell Signaling Technology; mouse monoclonal mAb 5A8 ($hCgA_{R47-L57}$)
183 antibody [32] and rabbit polyclonal C-terminal CST pAb CT-CST ($hCgA_{P368-R373}$) [33] were generously
184 provided by Angelo Corti (IRCCS San Raffaele Scientific Institute, Milan, Italy).

185

186 **Determination of plasma CST.** A commercial mouse EIA kit (RayBiotech Life, GA) was used to
187 determine plasma CST and followed according to the manufacturer's protocol.

188

189 **Non-invasive tail-cuff measurement of blood pressure**. Systolic blood pressure (SBP) was
190 measured using the mouse and rat tail cuff blood pressure (MRBP) System (IITC Life Sciences
191 Inc. Woodland Hills, CA). Mice were restrained in plexiglass tubes and heated to 34°C for 10-15
192 min in individual warming chambers prior to BP measurement. The tails were placed inside
193 inflatable cuffs with a photoelectric sensor that measured tail pulses. The SBP was measured
194 over 6 separate days with an average of two values per day.

195

196 **Measurement of plasma cytokines.** Plasma cytokines were measured using U-PLEX mouse
197 cytokine assay kit (Meso Scale Diagnostics, Rockville, MD) via the manufacturer's protocol.

198

199 **Real Time PCR**

200 Total RNA from heart tissue was isolated using RNeasy Mini Kit and reverse-transcribed using
201 qScript cDNA synthesis kit. cDNA samples were amplified using PERFECTA SYBR FASTMIX L-
202 ROX 1250 and analyzed on an Applied Biosystems 7500 Fast Real-Time PCR system. All PCRs
203 were normalized to *Rplp0*, and relative expression levels were determined by the $\Delta\Delta C_t$ method.

204

205 **Flow cytometry analysis**

206 Mouse heart perfusion was performed as previously described [34]. Cardiac stromal cells were
207 stained with fluorescence-tagged antibodies to detect macrophages ($CD11b^+F4/80^+$). Data were
208 analyzed using FlowJo software.

209

210 **Tissue macrophage depletion study.**

211 To deplete tissue macrophages, mice were given clodronate liposomes (50 mg/kg body weight;
212 catalog F70101C-N, FormuMax, Sunnyvale, CA) every 3 days via intraperitoneal injection. Mice
213 treated with control liposomes were used as control.

214

215 **Bone marrow transplantation.**

216 To generate irradiated chimeras, 10-12 weeks old WT or CST-KO NCD recipient mice received
217 a lethal dose of 10 Gy radiation, followed by tail vein injection of 2×10^6 bone marrow cells from
218 either WT or CST-KO NCD donor mice. After 16 weeks of bone marrow transplantation, all mice
219 were subjected to non-invasive tail-cuff measurement of BP.

220

221 **Transmission Electron Microscopy (TEM) and morphometric analysis.** To displace blood
222 and wash tissues before fixation, mice were cannulated through the apex of the heart and
223 perfused with a Ca^{2+} and Mg^{2+} free buffer composed of DPBS, and 9.46 mM KCl (to arrest hearts
224 in diastole), as described previously [35]. Fixation, embedding, sectioning and staining were done
225 following our previous publication [35]. Grids were viewed using a JEOL JEM1400-plus TEM (JEOL,
226 Peabody, MA) and photographed using a Gatan OneView digital camera with 4k x 4k resolution
227 (Gatan, Pleasanton, CA). Morphometric analysis of glycogen granules and cristae surface area
228 were determined as described previously by us [35].

229

230 **Microarrays.** Total RNA from left ventricular tissue from four CST-KO and age-matched WT mice
231 was isolated using a RNeasy Kit. RNA quality was assessed by using the Agilent Model 2100

232 Bioanalyzer. RNA was labeled and hybridized to a Nimblegen mouse 12-plex array. Array was
233 scanned on a GenePix 4000B scanner and data extracted using Arraystar 4. Raw data was
234 analyzed using a Bayesian variance modeling approach in VAMPIRE using a FDR of 0.05 [36].
235 Data were visualized using GeneSpring 14.5. Microarray data is available at GEO Accession
236 Number (GSE104071).
237
238 ***In vivo* tissue glucose uptake and metabolism.** *In vivo* glucose uptake and production of
239 glucose-6-phosphate (G6P) and glycogen was assessed following a published protocol but using
240 double isotopes - ^{3}H-glucose and ^{14}C-2-deoxyglucose (2DG) as described previously by us [35].
241
242 ***In vivo* fatty acid incorporation and lipid extraction and oxidation.** A 100 µl solution of U-^{14}C-
243 palmitic acid-BSA complex (molar ration 2.5:1), containing 1 µCi and 250 µM palmitate was
244 injected per mouse. After 90 min, mice were sacrificed, blood was saved and tissues were
245 subjected to lipid extraction by Bligh and Dyer's adaptation [37] of Folch's original method [38].
246 Radioactivity in the lower chloroform layer was determined by measuring fatty acids in the
247 aqueous layer by determining acid soluble metabolites (ASM, representing fatty acid oxidation)
248 as described previously by us [39].
249
250 **Determination of tissue glycogen.** Glycogen was extracted from the left ventricle by boiling with
251 30% KOH, precipitation by alcohol and determination with anthrone reagent [40].
252
253 **Langendorff perfused heart model.** Mice were anesthetized with sodium pentobarbital (50
254 mg/kg i.p.), the heart was excised and the aorta was cannulated for Langendorff perfusion of the
255 coronary circulation, as described previously [41]. For the ischemic preconditioning (IPC) protocol
256 the stabilization period was followed by two cycles of ischemia (5 min, no pacing) and reperfusion
257 (5 min, pacing after 1 min re-perfusion).
258
259 **Measurement of catecholamines:** Mice were anesthetized by inhalation of isoflurane and blood
260 was collected from the heart in potassium-EDTA tubes. Adrenal and plasma catecholamine were
261 measured using 3-CAT Research ELISA kit (LDN Immunoassays and Services, Nordhorn,
262 Germany).
263
264 **Statistics.** Statistics were performed with SPSS Statistics (IBM Corp., Armonk, NY). Data were
265 analyzed either with a Repeated Measure (RM) 2x2 ANOVA, 2-way ANOVA, UNIANOVA, and

subjected to post-hoc tests and pairwise comparisons where appropriate. Additionally, we performed unpaired student's t-test or Mann-Whitney U test depending on Shapiro-Wilk's test of normality (with results corrected for Levene's test for Equality of Variances where appropriate). All data are presented as mean ± SEM and significance was assumed when $p<0.05$.

271 **Results**

272 **Generation and validation of CST-KO mice.** Our strategy (see **Fig 1; S1**) for the development
273 of CST-KO mice involved a targeted elimination of the CST domain (63 bp) from Exon VII of the
274 *Chga* gene. CST-KO mice were expected to express truncated CgA but not CST. We confirmed
275 this by western blot analyses of lysates prepared from adrenal glands. The presence of CgA was
276 confirmed using a mouse monoclonal antibody (mAb 5A8) [32] (**Fig. 1B**) and a CgA ELISA (**Fig.**
277 **1D**); however, blots using a polyclonal antibody directed against the 6 C-terminal domains of CST
278 (pAb CT-CST) [33] showed a proteolytically processed CgA of ~46 kDa corresponding to $mCgA_{1-}$
279 $_{385}$ in WT littermates, but not in CST-KO mice (**Fig. 1C**). Because this antibody detected synthetic
280 CST (a positive control, indicating specificity of the antibody) we conclude that CST-KO mice
281 indeed lack CST (**Fig. 1C**). Analyses of levels of CST in the plasma from these mice further
282 confirmed the complete absence of CST in CST-KO mice (**Fig. 1E**).

283

284 **CST-KO mice are hypertensive and have enlarged and inflamed hearts; key phenotypes**
285 **are reversed by supplementation with recombinant CST.** We checked several cardiovascular
286 parameters that are expected to be affected by the lack of CST. We found that CST-KO hearts
287 are ~27% heavier than WT mice (**Fig. 1F&G**) and that the mice are hypertensive (**Fig. 1H**). These
288 findings indicate that heart structure and function are regulated by CST.

289 Next, we checked plasma CST level before and after treatment with exogenous
290 recombinant CST. In WT mice, plasma CST level was 0.86 nM, which increased to 1.72 nM 24
291 hr after treatment with exogenous CST (**Fig. 2B**). In CST-KO mice, plasma level of CST was
292 undetectable at baseline, as expected, and rose to 1.17 nM after supplementation (**Fig. 2B**).
293 These findings indicate that the supplementation of CST-KO mice with CST provides near
294 physiological concentration of CST. Through a series of studies, we next examined the
295 phenotypes of CST-KO mice and asked whether CST supplementation can restore some of the
296 key phenotypes.

297 First, we found that CST-KO mice show increased levels of proinflammatory plasma
298 cytokines including TNFα, IFNγ, MIP1α, MCP1, and KC/GRO (**Fig. 2C**). By contrast, anti-
299 inflammatory cytokine IL10 is decreased in CST-KO mice (**Fig. 2C**). CST treatment decreased
300 plasma proinflammatory cytokines and increased anti-inflammatory IL10 in both WT and CST-KO
301 mice (**Fig. 2C**). These findings in plasma cytokine levels were consistent with transcripts in the
302 heart muscle, as determined by qPCR-- CST-KO mice showed a reduction in several anti-
303 inflammatory markers (*IL4*, *Arg1*, *Clec7a* and *Clec10a*) (**Fig. 2D**) and a concomitant increase in
304 several other pro-inflammatory markers (**Fig. 2E**). These findings show that the balance between

305 pro- and anti- inflammatory pathways was skewed towards inflammation in CST-KO mice.
306 Exogenous CST supplementation reversed this disbalance; it induced several anti-inflammatory
307 pathways (**Fig. 2D**) and either normalized or markedly decreased proinflammatory cytokine
308 mRNA levels (**Fig. 2E**). These findings in the heart muscle and the plasma show that CST is both
309 necessary and sufficient for restoring immune homeostasis in the heart and in the systemic
310 circulation, respectively. The findings are also in accordance with CST's role as an anti-
311 inflammatory peptide [42-45].
312 Second, we checked the systolic BP (SBP) in these mice: High BP in CST-KO mice was
313 reduced to WT level after supplementation with CST (**Fig. 3A-B**). These findings demonstrate
314 that CST is necessary and sufficient for BP homeostasis and are consistent with the previously
315 described anti-HTN functions of CST [30, 46]. In addition, the finding that CST-KO mice display a
316 proinflammatory hypertensive phenotype is also consistent with prior studies showing that
317 proinflammatory cytokines (IL6) increase BP [47-49] and anti-inflammatory cytokines (IL2 and IL10)
318 decrease BP [50 51-54].
319 Third, we analyzed the microarchitecture of the heart: In the saline-treated WT mice,
320 Transmission Electron Microscopic (TEM) micrographs showed resident macrophages in the
321 inter-sarcolemmal spaces (**Fig. 3C**). In contrast, the saline-treated CST-KO heart showed a
322 marked infiltration of monocyte-derived macrophages (**Fig. 3C**), indicating inflammation of the
323 CST-KO heart. While treatment of WT mice with CST did not change the resident macrophage
324 population, CST-KO mice showed almost complete disappearance of infiltrated macrophages
325 after CST substitution (**Fig. 3F**). This was supported by FACS analysis showing ~38% decrease
326 of $CD11b^{+}F4/80^{+}$ macrophages in CST-supplemented CST-KO heart (**Fig. 3D**). These findings
327 reveal that CST is required for cardiac homeostasis and its absence is permissive to cardiac
328 inflammation.
329
330 **Macrophages are key effector cells responsible for the anti-inflammatory actions of CST.**
331 Next, we explored the implications of infiltrated macrophages in the hearts of CST-KO mice and
332 its relevance to cardiovascular physiology using two independent approaches (**Fig. 3A**). First, we
333 depleted macrophages by chlodronate (CDN) liposomes, which not only depleted resident and
334 infiltrated macrophages but also reversed the HTN phenotype of CST-KO mice (**Fig. 3G&H; S2**).
335 Because CDN did not reduce BP in WT mice, these findings show that macrophages may not be
336 required for normal cardiac functions, but its dysregulation (increased infiltration and/or aberrant
337 activation) may be a key contributor of the HTN phenotype in CST-KO mice.

338 Second, we carried out bone marrow transplantation (BMT) assays in which, we irradiated
339 both WT and CST-KO mice and then cross-transplanted their marrows-- CST-KO bone marrow
340 was transplanted into WT mice and *vice versa*. To our surprise, we found that BMT could transfer
341 the hypertensive phenotype-- while CST-KO-marrow recipient WT mice showed increased BP,
342 WT-marrow recipient CST-KO mice showed decreased BP (**Fig. 3I**). These findings indicate that
343 paracrine secretion of CST and/or cytokines by macrophages may regulate BP.
344 To confirm if CST is responsible for the observed BMT-induced phenotype switch, we
345 analyzed plasma CST and found that CST-KO mice who received WT-marrow, but not CST-KO-
346 marrow had near physiologic levels of CST in their plasma (0.52 nM) (**Fig. 3J**). These findings
347 suggest marrow-resident immune cells and/or hematopoietic system are a major contributor of
348 circulating CST in the plasma. They may do so either directly [through paracrine secretion from
349 macrophages, as observed in the case of serum cytokines (**Fig. 2C**)] or indirectly (perhaps *via*
350 other immune cells that feedback and regulate macrophage response).
351 Regardless, our studies using CDN and BMT implicate the macrophages and the innate
352 immune system as key effectors of the anti-hypertensive actions of CST. In the absence of CST
353 (as in CST-KO mice), macrophages are hyperactive and support both systemic (**Fig. 2**) and local
354 cardiovascular inflammation (**Fig. 3**) and trigger systemic HTN.
355
356 **Microarray studies reveal that CST impacts core bioenergetic and metabolic functions of**
357 **the myocardium.** To gain insights into the nature of the immunoendocrine actions of CST on the
358 heart, next we carried out transcriptomic analyses (gene microarray) of the left ventricles of WT
359 and CST-KO. Analysis revealed 437 genes with altered expression, up- or downregulated (false
360 discovery rate <0.05), as shown in the form of a heatmap (**Fig. 4A**).
361 Downregulated genes, which were most enriched in pathways that impact muscle
362 conduction and contractility (**Fig. 4B**) include, among other genes, *Glo1* (encodes glyoxylase I
363 enzyme that detoxifies methylglyoxal, which is a cytotoxic byproduct of glycolysis). Upregulated
364 genes include, among others, *Gm7120* (encodes predicted gene 7120 that acts as a hypercapnia
365 responsive gene), *Astn2* (encodes astrotactin 2 that functions as a lipid raft), and *Defa20*
366 (encodes defensin α-20 that exerts antibacterial humoral response) genes.
367 We validated several of these up- and downregulated genes by qPCR and found that CST
368 supplementation reversed these aberrant expressions in all cases, i.e., downregulated what was
369 aberrantly overexpressed or upregulated what was aberrantly suppressed (**Fig. 4C**). Of note,
370 *Glo1* in macrophages metabolizes methylglyoxal, an inflammatory agent whose accumulation
371 promotes vascular damage in HTN and diabetes. Therefore, it is possible that CST attenuates

372 inflammation and improves cardiovascular health in part through the regulation of *Glo1*
373 expression.
374 Targeted qPCR analyses of sarcomeric genes revealed reduced expression of *Tnni3*
375 (encodes cardiac troponin I, which helps to coordinate the contraction of the heart), *Tnnt2*
376 (encodes cardiac troponin T, which helps coordinate cardiac contraction), *Myl4* (encodes atrial
377 light chain-1 and is associated with atrial fibrillation) and *Myl7* (encodes atrial light chain-2 and
378 modulates cardiac development and contractility) genes in CST-KO mice (**Fig. 4D**). CST
379 treatment increased expression of *Tnni3*, *Tnnt2*, *Actc1* (encodes cardiac α-actin that is a major
380 constituent of the cardiac contractile apparatus), *Myl4* and *Myl7* genes in both WT and CST-KO
381 mice albeit to a much higher level in CST-KO mice (**Fig. 4D**).
382 *Tpm* (encodes tropomyosin protein that binds to actin filament and regulates cardiac
383 contraction) and *Ttn* (encodes titin protein, which interacts with actin and myosin and regulate
384 cardiac contraction) genes were not affected by the presence or absence of CST.
385 An analysis of mitochondrial genes revealed reduced expression of *Ndufa3* (nuclear-
386 encoded NADH-ubiquinone oxidoreductase 1 alpha subcomplex 3 of Complex I), *Sdhc* (nuclear-
387 encoded succinate dehydrogenase complex subunit C that is a subunit of Complex II) and *Atp5j*
388 (encodes mitochondrial membrane ATP synthase subunit 6 of Complex V, which produces ATP
389 from ADP) genes in CST-KO mice (**Fig. 4E**). CST treatment increased the expression of all three
390 genes in WT and CST-KO mice (**Fig. 4E**).
391 Taken together, these unbiased approaches and qPCR validation studies provide insights
392 into how an inflamed dysfunctional heart in the absence of CST may impact some of the core
393 fundamental functions of this vital organ by affecting its ultrastructure, muscle function
394 (contractility), rhythm, mitochondrial bioenergetics and conduction.
395
396 **CST-KO mice display a cardiometabolic shift: glucose utilization is decreased with a**
397 **concomitant increase in the utilization of fatty acids and insulin resistance.** We next asked
398 how CST may impact metabolism. Prior studies have shown that the heart is an omnivore, which
399 consumes fat, carbohydrate, protein, ketone bodies, or lactate [55], generating ~95% of total energy
400 via oxidation of fatty acids and glucose [56, 57]. Because diabetic hearts shift away from the utilization
401 of glucose [58], relying almost completely on fatty acids as an energy source, we looked at cardiac
402 metabolism in CST-KO mice, which we recently reported to be insulin-resistant [42]. CST-KO mice
403 showed decreased uptake of 2DG in LV compared to WT mice (**Fig. 5A**). Furthermore, G6P
404 utilization was significantly lower in CST-KO compared to WT (**Fig. 5A**). No significant difference
405 between CST-KO and WT was seen in generation of G6P (**Fig. 5A**).

406 We next looked at the mRNA levels of key genes involved in glucose metabolism. Thus,
407 we found decreased mRNA expressions of *Glut4* (encodes glucose transporter 4), *Pfkm* (encodes
408 the muscle isoform of phosphofructokinase, which catalyzes the irreversible conversion of
409 fructose-6-phosphate to frustose-1,6-bisphosphate) and *Pdk2* (encodes pyruvate dehydrogenase
410 protein kinase-2 that phosphorylates and inhibits pyruvate dehydrogenase activity resulting in
411 decreased glucose utilization and increased fat metabolism) in CST-KO mice compared to WT
412 mice (**Fig. 5B**), which corroborate with the biochemical findings.
413 Since plasma insulin level of CST-KO mice was higher than WT mice [42], poor glucose
414 metabolism correlate with reduced insulin sensitivity in CST-KO mice. CST supplementation
415 improved glucose uptake and utilization in CST-KO mice (**Fig. 5A**), indicating CST has an insulin-
416 like activity or CST is an insulin-sensitizing peptide. We also found that compared to WT mice,
417 CST-KO mice show a significant higher FA uptake (**Fig. 5C**). This could be due to the higher
418 plasma insulin level in CST-KO mice [42] that drives increased lipid metabolism (but not higher
419 glucose metabolism due to insulin resistance). Furthermore, ^{14}C-labeled acid soluble metabolites
420 (ASM) were significantly higher in CST-KO compared to WT mice (**Fig. 5C**). These findings
421 suggest that increased dependence on fatty acids for energy needs make CST-KO hearts
422 resistant to insulin.
423 We confirmed these biochemical findings by analyzing the levels of expression of key
424 genes involved in lipid metabolism. We found increased mRNA levels of fatty acid transporter
425 *Cd36* (encodes cd36 antigen, which is scavenger receptor, and functions in high affinity tissue
426 uptake of long-chain fatty acids) and *Slc27a1 (FATP1)* (encodes long-chain fatty acid transporter
427 1, which transports long-chain fatty acids in an ATP-dependent manner) as well as of the enzyme
428 for triglyceride formation *Dgat2* (encodes diacylglycerol O-acyltransferase 2 enzyme, which
429 catalyzes the terminal step in triacylglycerol synthesis), and the transcription factor *Pparα,* which
430 supports fatty acid oxidation (**Fig. 5D**). In addition, we found increased expression of *Sptlc1*
431 (encodes serine palmitoyltransferase enzyme, which catalyzes the 1st step in sphingolipid
432 biosynthesis) and *Cers2* (encodes ceramide synthase 2 enzyme, which catalyzes the synthesis
433 of very long acyl ceramides, including C20 and C26 ceramides) genes (**Fig. 5D**), indicating
434 increased ceramide synthesis, which will make the CST-KO heart more resistant to insulin.
435 In contrast, CST treatment decreased expression of *Cd36*, *Dgat2*, *Sptl1c*, *Cers2* and
436 *Ppara* (key regulator of lipid metabolism) genes. These findings indicate that CST improved
437 metabolic health of the CST-KO heart by converting them from insulin-resistant to insulin-
438 sensitive. Next, we checked the status of glycogen (readily mobilized storage form of glucose).
439 We found low glycogen storage in 'Fed' CST-KO heart compared to 'Fed' WT mice. CST

440 supplementation improved glycogen storage in both WT and CST-KO heart (**Fig. 5E**). The
441 biochemical findings were supported by morphometric analyses of glycogen granules in EM
442 micrographs (**Fig. 5F&G**).
443 Furthermore, because increased accumulation of fatty acids, diacylglycerol, and ceramide
444 impairs insulin signaling [59], we also evaluated the hearts from WT and CST-KO mice for
445 phosphoproteins (e.g., AKT and GSK-3β) within the insulin signaling cascades that are commonly
446 indicative of the metabolic effects of insulin. We found that the hearts from CST-KO mice had
447 reduced phosphorylation of AKT at ser473 site and GSK-3β at ser9 site (**Fig. 5H-J**), indicating
448 decreased insulin sensitivity. This phenotype was reversed upon CST treatment because both
449 phosphoproteins were restored in the hearts of CST-KO mice (**Fig. 5H-J**). These findings
450 reinforce CST as an insulin-sensitizing peptide in the heart, which is consistent with its previously
451 described role in other tissues [42, 60].
452 Taken together with the cardiometabolic shifts, these findings indicate that CST is a
453 hormone that maintains cardiometabolic homeostasis; it does so at least in part by acting as an
454 insulin-sensitizing peptide which regulates myocardial choice of substrate for generating energy
455 (i.e., ATP).
456
457 **The myocardium in CST-KO mice show mitochondrial dysfunction.** The myocardium relies
458 heavily on mitochondria for the generation of ATP and maintenance of intracellular Ca^{2+} fluxes [61].
459 Prior studies have shown that HTN is associated with structural mitochondrial abnormalities that
460 result in impaired energy production and accelerated formation of ROS through instability of
461 electron transport chain complexes [62, 63]. Because the hypertensive CST-KO mice showed gene
462 expression **(Fig. 4)** and biochemical **(Fig. 5)** profiles indicative of altered bioenergetics and
463 mitochondrial dysfunction, next we analyzed the mitochondria health in the WT and CST-KO
464 mice. To this end, we used TEM to analyze and resolve the two populations of mitochondria in
465 the heart-- the interfibrillar mitochondria (IFM) which align in longitudinal rows between myofibrils
466 and the subsarcolemmal mitochondria (SSM) that localize below the sarcolemma. These two
467 subpopulations have distinct respiration rates associated with different metabolic enzyme
468 activities, morphological structures, and lipid contents [64, 65]. Under low magnification we analyzed
469 the shape, location and orientation of SSM (**Fig. 6A-D**) and IFM (**Fig. 6I-L**). Under high
470 magnification we analyzed the shape and orientation of mitochondrial cristae [SSM (**Fig. 6E-H**)
471 and IFM (**Fig. 6M-P**)]. These morphometric analyses revealed significant reduction in cristae
472 surface area in CST-KO mice, which was rescued after CST supplementation (**Fig 6E-H; 6M-P**).

473 Because cristae shape and density determine the assembly and stability of respiratory
474 chain supercomplexes and efficiency [63], taken together with transcriptomic and biochemical
475 analyses the TEM findings showed that both mitochondrial structure and function are impaired in
476 the hearts of CST-KO mice.
477 Consistent with myocardial insulin resistance, CST-KO hearts showed accumulation of
478 lipid droplets, which are implicated in contractile and diastolic dysfunctions [66, 67]. Mitophagy, the
479 mitochondrial-specific analog of autophagy, represents breakdown of damaged and
480 malfunctioning mitochondria [68-70]. Mitophagy in CST-KO mice indicates impaired mitochondrial
481 function. CST supplementation improved cristae surface area, markedly reduced lipid
482 accumulation, and decreased mitophagy in CST-KO heart. These findings indicate that CST can
483 enhance cardiovascular functions by improving the health of mitochondria, and thereby
484 cardiomyocyte metabolism.
485
486 **Ischemic pre-conditioning-induced cardioprotection is severely impaired in CST-KO heart.**
487 We investigated the response of hearts from WT and CST-KO mice to ischemia/reperfusion (I/R)
488 and tested responses to ischemic preconditioning (IPC). For the functional measures 'LVDP
489 (mmHg)' (**Fig. S3A**), 'LVEDP (mmHg)' (**Fig. S3C**), 'dP/dt$_{max}$ (mmHg/sec.)' (**Fig. S3B**), 'dP/dt$_{min}$
490 (mmHg/sec.)' (**Fig. S3D**) revealed that IPC significantly increased post-ischemic LVDP and
491 lowered LVEDP in WT hearts compared to CST-KO hearts and their respective IR controls (**Fig**
492 **S3A&3C**). Furthermore, neither LVDP nor LVEDP was significantly modified in IPC treated CST-
493 KO hearts compared to respective IR controls. Sidak's pairwise comparison revealed that IPC
494 improved recoveries of both dP/dt$_{max}$ (**Fig. S3C**) and dP/dt$_{min}$ (**Fig. S3D**) compared to respective
495 IR controls. When compared to CST-KO mice, a moderate effect on dP/dt$_{max}$ and dP/dt$_{min}$ was
496 seen (few significant time-points during 45 min reperfusion). Furthermore, neither dP/dt$_{max}$ nor
497 dP/dt$_{min}$ was increased significantly in IPC treated CST-KO hearts compared to respective IR
498 controls. Detailed values for pair-wise comparisons are included in a supplementary table.
499 In aggregate, these data show CST-KO mice could not be preconditioned to the extent
500 seen in WT mice. WT mice were protected with IPC, with observed improvements in all functional
501 measures in the re-perfusion period, while CST-KO mice showed only marginal improvements.
502
503 **CST-KO adrenal medulla is populated with infiltrated macrophages and heightened**
504 **sympathetic stimulation with consequent hypersecretion of catecholamines.** Because prior
505 studies have implicated altered CA secretion from an inflamed adrenal medulla in progression of
506 HTN [3, 4], we next evaluated the adrenal glands in the CST-KO mice. TEM studies revealed that

507 compared to WT littermates, CST-KO mice had an abundance of infiltrated macrophages in the
508 intercellular spaces of chromaffin cells (**Fig. 7A)**. Supplementation with CST reduced the
509 abundance of macrophage infiltrates in CST-KO mice, but did not affect the resident macrophage
510 population in the WT mice (**Fig. 7A**). By contrast, treatment with chlodronate resulted in complete
511 loss of macrophages (both resident and infiltrates) in both WT and CST-KO mice (**Fig. 7A**).
512 Because prior studies in humans, mice and rats have shown that pro-inflammatory
513 cytokines such as IFNα [71, 72], IL1β [73, 74], and TNFα[75, 76] increase CAs production and secretion,
514 we asked if the inflamed adrenal glands in CST-KO mice produce and secrete more CAs. We
515 found that compared to WT littermates, both adrenal (**Fig. 7B**) and plasma (**Fig. 7C**) levels were
516 elevated in CST-KO mice. In addition, the CST-KO adrenal medulla exhibit abundant docked
517 chromaffin granules (CG) and decreased acetylcholine containing vesicles at the sympatho-
518 adreno-medullary synapse (**Fig. 7D&E**), implicating heightened sympathetic nerve activity
519 eventuating in hypersecretion of CA. Supplementation of CST-KO mice with CST not only
520 inhibited infiltration of macrophages in the adrenal medulla (**Fig. 7A**) but also had a concomitant
521 decrease in both plasma and adrenal CAs (**Fig 7B&C**).
522 These findings demonstrate that CST is necessary and sufficient to suppress CA
523 production and secretion and thereby exert its anti-HTN effect and orchestrate cardiometabolic
524 homeostasis. Findings also support the following working model for how CST may accomplish
525 these roles *via* two independent but synergistic mechanisms (see **Fig. 8**): (i) inhibiting the
526 infiltration of macrophages, thereby inhibiting paracrine cytokine regulation of CA production and
527 secretion, (ii) attenuating sympathetic nerve activity, thereby decreasing cholinergic stimulus for
528 secretion of CA.
529
530
531
532
533

534 **Discussion**

535

536 Previous studies showing low levels of CST in hypertensive subjects [20] and normalization of BP
537 in CgA-KO mice by CST [30] as well as decreasing BP in polygenic models of rodent HTN [46] indicate
538 that CST is sufficient to reverse HTN. The findings of hypertensive phenotype in CST-KO mice
539 and restoration of that phenotype by exogenous administration of recombinant CST establishes
540 that CST is both necessary and sufficient in regulating HTN. This precise experimental model
541 also uncovered three mutually interdependent mechanisms (discussed below) *via* which CST may
542 exert its anti-HTN and cardioprotective effects, and thereby, maintain cardiovascular
543 homeostasis.

544

545 **Immunoendocrine regulation of BP.** Cardiac macrophages are critical for myocardial
546 homeostasis [77-81]: while a subset of them orchestrate monocyte recruitment and contribute to
547 heart failure pathogenesis [82], another is increased during diastolic dysfunction [34], myocardial
548 infarction and acute hemodynamic stress [77, 83]. We found an abundance of infiltrated
549 macrophages in the hearts and the adrenal glands of CST-KO mice. Using two parallel
550 approaches (chlodronate and BMT) to decrease macrophage activity, we found that macrophages
551 are key effector cells for the anti-HTN actions of CST.

552

553 **Immune regulation of cardiometabolic homeostasis, mitochondrial structure and function.**
554 The regulation of heart function by immune cells is well documented [84, 85]. Although myocardial
555 dysfunctions in rodents[86] and humans [87, 88] have been associated with increased TNFα
556 production, how inflammation may reduce cardiac contractility and/or conduction, two of the most
557 important functions of the myocardium, remains poorly defined. Contractility of the myocardium
558 requires ATP [89], ~6 kg of ATP/ d, which is ~20 times its own weight [90-93], produced predominantly
559 *via* oxidative phosphorylation in the mitochondria and, to a lesser extent, by glycolysis [94].
560 Therefore, mitochondrial health is critical for the proper functioning of the heart. A plethora of
561 substrate are used to produce ATP, including fatty acids, glucose, some amino acids, lactate, and
562 ketones [55, 95] and substrate selection depends largely on substrate availability, oxygen
563 concentration and myocardial workload [96, 97]. Under normal conditions, the heart relies
564 predominantly (~60-90%) on fatty acid (FA) oxidation to fuel ATP production, whereas the
565 remaining ~10-40% of ATP is derived from pyruvate oxidation [98]. Metabolic flexibility (the capacity
566 of the healthy heart to shift between different substrates to ensure a continuous output of energy)
567 is established as a crucial feature of cardiac energy metabolism [99]. Such flexibility was lost in

568 CST-KO mice because hearts in these mice showed increased FA uptake and oxidation coupled
569 with decreased glucose uptake and oxidation in CST-KO mice; these changes have been
570 reported in insulin-resistant and diabetic rodents [100-102] and is a distinctive feature in obesity-
571 associated metabolic diseases in humans [103-105]. Such metabolic inflexibility, was reversed by
572 supplementation of CST-KO mice with CST, underscoring that CST is necessary and sufficient
573 for cardiometabolic homeostasis and flexibility.

574 As for how CST may regulate the cardiometabolic state, we found that mitochondrial
575 structure and function were altered in its absence and restored by exogenous supplementation of
576 CST. These findings are consistent with prior studies showing that HTN is associated with
577 decreased mitochondrial mass and density, increased mitochondrial swelling, impaired energy
578 production and the accelerated formation of reactive oxygen species (ROS) [62]. In addition, HTN
579 rats display mitochondrial fragmentation and increased ROS production [106].

580 In congruence with increased FA uptake in the setting of decreased mitochondrial
581 oxidative capacity, CST-KO mice displayed intramyocardial lipid droplets; such droplets are
582 normally found in an obese and diabetic heart [107-109] and are known to trigger mitochondrial
583 dysfunction and energetic compromise eventuating in cardiac dysfunctions [104, 110, 111]. In addition,
584 like a diabetic heart, myocardial insulin resistance (decreased phosphorylation of AKT and GSK-
585 3β) and impaired glucose utilization (decreased glucose uptake and oxidation) in CST-KO mice
586 resulted in a further increase in cardiac FA uptake and accumulation of toxic lipid metabolites
587 including triacylglycerol, diacylglycerol and ceramide [112-114]. Of note, inflammatory cytokines like
588 TNFα induces synthesis of ceramides, linking immune cells in induction of ceramide synthesis
589 [115]. We have previously shown that CST markedly decreases triglyceride, FA and ceramides in
590 diet-induced obese (DIO) liver and improves insulin sensitivity in CST-KO and DIO mice [42]. CST
591 supplementation in CST-KO mice results in the development of the following phenotypes: (i)
592 increased glucose uptake and metabolism, (ii) decreased FA uptake and oxidation, (iii) decreased
593 accumulation of lipid droplets, and finally, (iv) decreased mitophagy. These findings underscore
594 the crucial roles that CST plays in improvement of cardiac metabolism and function.
595

596 **Neuro-adrenergic overdrive-induced HTN and immunoendocrine regulation of BP.** Existing
597 literature reveals heightened sympathetic nerve activity (SNA) in white coat and borderline
598 hypertensive subjects [116, 117], and the magnitude of the elevation of SNA is related to the
599 magnitude of hypertension [118, 119]. Like humans, SHR shows reduced cardiac parasympathetic
600 nerve activity, elevated SNA and increased NA release [120, 121]. Here, we found neuro-adrenergic
601 overdrive-induced HTN in CST-KO mice. Augmented SNA in HTN is known to activate both

602 myeloid cells and T cells [11, 122], and primary HTN shows increased circulating concentration of
603 proinflammatory cytokines such as TNFα and IL6 [123]. To our knowledge, the present study is the
604 1st to demonstrate increased infiltration of macrophages in the adrenal medulla concomitant with
605 increased secretion of CAs and the consequent development of HTN in CST-KO mice, which
606 were normalized after CST supplementation. These findings imply that CST regulates BP through
607 a novel immunoendocrine regulation of CA secretion.
608

609 **Acknowledgments:**
610 Supported by grants from the Veterans Affairs (I01 BX003934 to SKM; BX001963 to HHP) and
611 the National Institutes of Health (AI141630 to P.G, GM138385 to D.S and HL091071, HL066941,
612 AG053568, AG052914, AG052722 to HHP).
613

614 **Author contributions:**
615 W.Y., designed and generated CDN liposome, bone marrow transplantation and FACS analyses
616 data. Provided inputs and edited the MS.
617 K.T., designed and generated qPCR, plasma cytokine, CgA and CST in tissue and plasma, and
618 catecholamines in tissue and plasma data. Provided inputs and edited the MS.
619 E.A., designed and generated western blot data. Edited the MS.
620 J.M.S., designed and generated ischemia reperfusion and ischemic pre-conditioning data as well
621 as made statistical analyses of the data.
622 T.P. and G.B., designed and generated glucose and fatty acid uptake and oxidation data.
623 M.A.L., generated blood pressure data. Edited the MS.
624 S.M., generated qPCR data and edited the MS.
625 S.D., Intellectual input in the analysis of the CST-KO immunophenotype (gene expression and
626 reactome pathway).
627 H.H.P., supervised ischemia reperfusion and ischemic pre-conditioning studies and provided
628 financial support for those studies.
629 N.J.G.W., designed and generated microarray data and edited the MS
630 D.S., Analyzed and interpreted the microarray dataset, generated heat map.
631 P.G., Extensively edited the MS and Figures, interpreted transcriptomic dataset, made Figures
632 and provided crucial inputs on the overall organization of the MS and Figures.
633 S.K.M., conceived the idea, generated TEM data, supervised >90% of the studies, analyzed the
634 data and made the graphics with extensive inputs from P.G., wrote the MS with extensive inputs
635 from P.G. and provided financial support (>95%).

636

637

638 **Disclosures:**

639 None

640

642 **Figure legends**

643 **Fig. 1. CST-KO mice have enlarged hearts.**

644 **(A) Schematic diagram showing the cloning strategy for generating CST-KO mice. (B)**
645 **Western blot showing the presence of CgA in the left ventricle of WT and CST-KO mice.**
646 Mouse monoclonal antibody 5A8 detects full-length CgA (~70 kDa). While WT mice showed a
647 band of ~70 kDa, CST-KO mice showed a proteoglycan form of CgA. **(C) Western blot showing**
648 **the presence of CgA and CST.** A rabbit polyclonal antibody against the C-terminal domain of
649 CST (P_{368}-R_{373}) detects CST as well as CgA up to CgA_{1-373}. In the WT mice, this antibody detected
650 a proteolytically processed CgA (~45 kDa spanning CgA_{1-373}) and detected no band in CST-KO
651 mice, confirming deletion of CST domain. **(D). Graph display adrenal CgA.** A commercial mouse
652 EIA kit (CUSABIO Technology LLC, Houston, TX) was used to determine adrenal CgA content in
653 WT and CST-KO mice. **(E) Graph display plasma CST (n=6).** A commercial mouse EIA kit
654 (RayBiotech Life, GA) was used to determine plasma CST level in WT and CST-KO mice. **(F)**
655 **Size of wet heart.** Hearts were dissected out from WT and CST-KO mice and placed on top of a
656 piece of paper. Photographs show bigger heart in CST-KO mice compared to WT mice. **(G)**
657 **Weight of wet heart (n=16).** CST-KO wet heart was 27.5% heavier than WT heart when
658 normalized to body weight. **(H) Systolic BP (n=12).** SBP in WT and CST-KO mice. A tail-cuff
659 method (MRBP, IITC Inc. Life Science, CA) was used to determine SBP. DTA, diphtheria toxin;
660 FRT, *Flp* recognition target. ***p<0.001.

661

662 **Fig. 2. CST-KO mice are hypertensive, display systemic and cardiac inflammation; all**
663 **phenotypes are reversed by exogenous CST (2 µg/g body weight for 3 weeks).**

664 **(A) Schematic diagram** showing the interventional studies done on mice. **(B) Plasma CST** after
665 saline or 24 hr of CST treatment (n=6). The EIA kit used in Fig 1D above was used to measure
666 plasma CST **(C) Plasma cytokines** in saline or CST treated WT and CST-KO mice (n=8). U-
667 PLEX mouse cytokine assay kit (Meso Scale Diagnostics, Rockville, MD) was used to determine
668 plasma cytokine levels. **(D) RT-qPCR data** showing steady-state mRNA levels of anti-
669 inflammatory cytokines in left ventricle (n=8). Note increased expression of anti-inflammatory
670 genes in CST-KO mice after 3 weeks of treatment with CST. In WT mice, CST treatment caused
671 increased expression of *IL10*, *Mrc1* and *Arg1 genes*. **(E) RT-qPCR data** showing steady-state
672 mRNA levels of proinflammatory cytokines in left ventricle (n=8). Note increased mRNA levels of
673 proinflammatory genes in saline-treated CST-KO mice. Treatments of CST-KO mice with CST
674 caused significant decrease in mRNA levels. Ns, not significant; *p<0.05; **p<0.01; ***p<0.001.

675

676 **Fig. 3. Macrophages are key mediators of the proinflammatory cardiovascular phenotypes**
677 **in the CST-KO mice.**
678 **(A) Schematic diagram showing the interventional studies done on mice. (B) Systolic blood**
679 **pressure (SBP)** after saline or 3 weeks of CST treatment. A tail-cuff method (MRBP, IITC Inc.
680 Life Science, CA) was used to determine SBP in saline or CST-treated conscious mice. **(C, F&G)**
681 **Ultrastructural demonstration** of macrophages in WT and CST-KO heart (n=4). **(C) Saline-**
682 **treated** WT and CST-KO heart. Note the presence of none or a single resident macrophage **in**
683 WT heart and infiltrated macrophages in CST-KO heart. **(D) FACS data** showing macrophage
684 population in CST-KO heart after treatment with saline or CST (n=3). **(E) Bar graph** showing
685 CD45+ leukocytes in CST-KO mice in presence or absence of CST. **(F) CST-treated WT and**
686 **CST-KO heart**. Note the presence of only resident macrophages. **(G) Chlodronate (CDN)-**
687 **treated** WT and CST-KO heart. Note complete absence of macrophages. **(H) SBP** after depletion
688 of macrophages by CDN (n=8). Note significant decrease (by 36 mmHg) in BP after CDN. **(I) SBP**
689 after bone marrow transplantation (BMT) into irradiated mice (n=8). Note increased BP in WT
690 mice after receiving CST-KO-BMT and decreased BP in CST-KO mice after receiving WT-BMT.
691 **(J) Plasma CST** in BMT mice (n=6). Note macrophage-derived CST in CST-KO mice that
692 received WT-BMT. IFM, intermyofibrillar mitochondria; Mϕ, macrophage; ns, not significant; SSM,
693 sub-sarcolemmal mitochondria; *p<0.05; **p<0.01; ***p<0.001.
694
695 **Fig. 4. Analysis of cardiac transcripts in CST-KO mice reveal defects in the core myocardial**
696 **functions.**
697 **(A) Gene array data** showing differential expression of genes (log2) in WT and CST-KO mice
698 (n=5). **(B) RT-qPCR data** validating gene array data as well as expression after CST
699 supplementation (n=6). (**C**) **Expression of sarcomere genes** in WT and CST-KO mice after
700 treatment with saline or CST (n=6)**. (F) Expression of mitochondrial genes** in WT and CST-KO
701 mice after treatment with saline or CST (n=6). Ns, not significant; *p<0.05; **p<0.01; ***p<0.001.
702
703 **Fig. 5. CST-KO mice display an altered cardiometabolic phenotype, insulin resistance**
704 **(A) 2-deoxy-glucose (2DG) uptake and gluclose-6-phosphate (G6P) utilization** 90 min after
705 2DG injection (n=6). **(B) Relative expression of genes involved in glucose metabolism (n=6).**
706 **(C) Fatty acid (palmitic acid) uptake and oxidation (acid soluble metabolite: ASM)** 90 min
707 after injection of palmitic acid (n=6). (**D**) **Relative expression of genes involved in fat**
708 **metabolism and fat metabolites (n=6). (E) Cardiac glycogen** level in WT and CST-KO mice
709 after treatment with saline or CST (n=6). **(F) Morphometric analyses** of glycogen granules. **(G)**

710 Ultrastructural demonstration of glycogen granules (GG) in ventricle of WT and CST-KO mice
711 after treatment with saline or CST. **(H) Immunoblot data (n=4).** Representative western blots (12
712 hr fasting; n=4) from left ventricle of 4 mice in each group. **(I&J)** Densitometric values: **(I)** AKT
713 and **(J)** GSK-3β. Ns, not significant; *p<0.05; **p<0.01; ***p<0.001.
714
715 **Fig. 6. CST-KO mice display altered mitochondrial morphology**
716 **Transmission Electron Microscopic (TEM) images showing mitochondria and cristae (n=4).**
717 **(A-D) Low magnification micrographs** showing sub-sarcolemmal mitochondria (SSM). Note the
718 presence of mitophagy (Mp) in saline-treated CST-KO mice **(C),** which was abolished after
719 treatment with CST **(D). (E-H) High magnification micrographs** showing SSM. Note broken and
720 smaller cristae in saline-treated CST-KO mice **(G),** which were restored after treatment with CST
721 **(H). (I-L) Low magnification micrographs** showing inter- or intramyofibrillar mitochondria (IFM).
722 Note the presence of lipid droplets (LD) juxtaposed to IFM in saline-treated CST-KO mice **(L),**
723 which were dramatically reduced after treatment with CST **(L). (M-P) High magnification**
724 **micrographs** showing IFM. Note broken and smaller cristae in saline-treated CST-KO mice **(O),**
725 which were restored after treatment with CST **(P). (Q) High magnification IFM** showing LD. **(R)**
726 **High magnification SSM** showing mitophagy (Mp). **(S) Morphometric data** showing decreased
727 cristae surface area in saline-treated CST-KO mice, which were restored in CST-treated CST-KO
728 mice. Ns, not significant; *p<0.05.
729
730 **Fig. 7. CST-KO mice display inflamed adrenal medulla and altered catecholamine secretion**
731 **TEM micrographs of the adrenal medulla (n=4). (A)** Low magnification micrographs showing
732 resident macrophage in WT mice and resident plus infiltrated macrophages in CST-KO mice in
733 presence or absence of CST or CDN. Note close association of macrophage with the axon
734 terminal (AT) of the splanchnic nerve in CST-KO mice, indicating crosstalk between macrophages
735 and synaptic vesicles. (**B) Adrenal catecholamines** (n=12). CST-KO mice store more
736 norepinephrine (NE) than WT mice. **(C) Plasma catecholamines** (n=12). Note increased plasma
737 DA, NE and epinephrine (EPI) levels in CST-KO mice, which were significantly reduced by
738 supplementation with CST. **(D)** High magnification micrographs showing chromaffin granules
739 (CG) in the adrenal medulla. Note docked CG in CST-KO mice. (**E**) High magnification
740 micrographs showing splanchnico-adrenomedullary synapse with clear acetylcholine vesicles
741 (AChV) and dense core peptidergic vesicles (PdV). CC, chromaffin cell; Mϕ, macrophage; ns, not
742 significant; *p<0.05; **p<0.01; ***p<0.001
743

744 **Fig. 8. Summary or findings and working model.**

745 Schematic showing the major conclusions from the current work and its relevance to human
746 cardiovascular health and HTN. Based on our findings in CST-KO mice, and prior work
747 demonstrating the association of SNPs in CST with HTN and CVD, we propose a model wherein
748 CST maintains cardiac homeostasis and prevents HTN *via* two major mechanisms-- First, it exerts
749 an anti-inflammatory action *via* its effect on macrophage processes and polarization. Second, it
750 exerts a negative feedback loop on CA secretion from chromaffin cells [13, 124, 125]. In the absence
751 of CST, serum CA (e.g., NE) is elevated and macrophages become reactive in phenotype. While
752 the former results in HTN, the latter causes inflammation in the adrenals and heart. Macrophage
753 infiltration in the heart and local secretion of cytokines by activated macrophages result in altered
754 myocardial ultrastructure, bioenergetics, cardiometabolic shift, insulin resistance, and core
755 myocardial functions, e.g., ischemic preconditioning related protection. In doing so, CST acts as
756 a central mediator of cardiovascular homeostasis *via* a complex immunoendocrine axis.
757

758 **Supplementary Figure Legends**

759

760 **Fig. S1. Screening of CST-KO mice by PCR.** Primer set 1 was designed flanking the
761 CST domain. CST-KO mice showed a PCR product of 162 bp compared to 225 bp in WT
762 mice. Reverse primer 2 was designed from the CST domain. Therefore, there will be no
763 PCR product in CST-KO mice when primer set 2 was used. The WT mice showed a
764 product of 180 bp.

765

766 **Fig. S2. Depletion of macrophages by clodronate liposomes.** The cardiac
767 macrophage population was evaluated by FACS analysis after treatment of clodronate
768 liposomes (n=4 mice per group). Cardiac macrophage: $CD45^{+}CD11b^{+}F4/80^{+}$.

769

770 **Fig. S3. IPC-induced cardioprotection against I/R injury.** Hearts were excised and
771 perfused on a Langendorff apparatus for I/R and IPC studies. **LVDP.** Changes in LVDP
772 are shown in **A** and **B**. We found a significant effect of time (p<0.001), and time * strain *
773 protocol (p=0.042), with no significant effect for time * strain, and time * protocol. **LVEDP.**
774 Changes in LVEDP are shown in **C** and **D**. There was a significant effect of time
775 (p<0.001), and time * strain * protocol (p<0.001), with no significant effect for time * strain,
776 and time * protocol. **dP/dt_{max}:** Changes in dP/dt_{max} are shown in **E** and **F**. There was a
777 significant effect of time (p<0.001), with no significant effect for time * strain, and time *
778 protocol, or time * strain * protocol. **dP/dt_{min}**. Changes in dP/dt_{min} are shown in **G** and **H**.
779 There was a significant effect of time (p<0.001), and time * protocol (p=0.004), with no
780 significant effect for time * strain, and time * strain * protocol.

781

782

References

1. Bromfield S, Muntner P. High blood pressure: The leading global burden of disease risk factor and the need for worldwide prevention programs. *Curr Hypertens Rep*. 2013;15:134-136
2. Forouzanfar MH, Liu P, Roth GA, Ng M, Biryukov S, Marczak L, Alexander L, Estep K, Hassen Abate K, Akinyemiju TF, Ali R, Alvis-Guzman N, Azzopardi P, Banerjee A, Barnighausen T, Basu A, Bekele T, Bennett DA, Biadgilign S, Catala-Lopez F, Feigin VL, Fernandes JC, Fischer F, Gebru AA, Gona P, Gupta R, Hankey GJ, Jonas JB, Judd SE, Khang YH, Khosravi A, Kim YJ, Kimokoti RW, Kokubo Y, Kolte D, Lopez A, Lotufo PA, Malekzadeh R, Melaku YA, Mensah GA, Misganaw A, Mokdad AH, Moran AE, Nawaz H, Neal B, Ngalesoni FN, Ohkubo T, Pourmalek F, Rafay A, Rai RK, Rojas-Rueda D, Sampson UK, Santos IS, Sawhney M, Schutte AE, Sepanlou SG, Shifa GT, Shiue I, Tedla BA, Thrift AG, Tonelli M, Truelsen T, Tsilimparis N, Ukwaja KN, Uthman OA, Vasankari T, Venketasubramanian N, Vlassov VV, Vos T, Westerman R, Yan LL, Yano Y, Yonemoto N, Zaki ME, Murray CJ. Global burden of hypertension and systolic blood pressure of at least 110 to 115 mm hg, 1990-2015. *JAMA*. 2017;317:165-182
3. Goldstein DS. Plasma catecholamines and essential hypertension. An analytical review. *Hypertension*. 1983;5:86-99
4. Floras JS. Epinephrine and the genesis of hypertension. *Hypertension*. 1992;19:1-18
5. Mathar I, Vennekens R, Meissner M, Kees F, Van der Mieren G, Camacho Londono JE, Uhl S, Voets T, Hummel B, van den Bergh A, Herijgers P, Nilius B, Flockerzi V, Schweda F, Freichel M. Increased catecholamine secretion contributes to hypertension in trpm4-deficient mice. *J Clin Invest*. 2010;120:3267-3279
6. Currie G, Freel EM, Perry CG, Dominiczak AF. Disorders of blood pressure regulation-role of catecholamine biosynthesis, release, and metabolism. *Curr Hypertens Rep*. 2012;14:38-45
7. Fisher JP, Paton JF. The sympathetic nervous system and blood pressure in humans: Implications for hypertension. *J Hum Hypertens*. 2012;26:463-475
8. Dzielak DJ. Immune mechanisms in experimental and essential hypertension. *Am J Physiol*. 1991;260:R459-467
9. Coffman TM. Under pressure: The search for the essential mechanisms of hypertension. *Nat Med*. 2011;17:1402-1409
10. Byrne CJ, Khurana S, Kumar A, Tai TC. Inflammatory signaling in hypertension: Regulation of adrenal catecholamine biosynthesis. *Front Endocrinol (Lausanne)*. 2018;9:343
11. Norlander AE, Madhur MS, Harrison DG. The immunology of hypertension. *J Exp Med*. 2018;215:21-33
12. Sesso HD, Buring JE, Rifai N, Blake GJ, Gaziano JM, Ridker PM. C-reactive protein and the risk of developing hypertension. *JAMA*. 2003;290:2945-2951
13. Mahata SK, O'Connor DT, Mahata M, Yoo SH, Taupenot L, Wu H, Gill BM, Parmer RJ. Novel autocrine feedback control of catecholamine release. A discrete chromogranin a fragment is a noncompetitive nicotinic cholinergic antagonist. *J Clin Invest*. 1997;100:1623-1633
14. Winkler H, Fischer-Colbrie R. The chromogranins a and b: The first 25 years and future perspectives. *Neuroscience*. 1992;49:497-528
15. Montero-Hadjadje M, Vaingankar S, Elias S, Tostivint H, Mahata SK, Anouar Y. Chromogranins a and b and secretogranin ii: Evolutionary and functional aspects. *Acta Physiol (Oxf)*. 2008;192:309-324

16. Bartolomucci A, Possenti R, Mahata SK, Fischer-Colbrie R, Loh YP, Salton SR. The extended granin family: Structure, function, and biomedical implications. *Endocr Rev*. 2011;32:755-797
17. Chen Y, Rao F, Rodriguez-Flores JL, Mahapatra NR, Mahata M, Wen G, Salem RM, Shih PA, Das M, Schork NJ, Ziegler MG, Hamilton BA, Mahata SK, O'Connor DT. Common genetic variants in the chromogranin a promoter alter autonomic activity and blood pressure. *Kidney Int*. 2008;74:115-125
18. O'Connor DT, Zhu G, Rao F, Taupenot L, Fung MM, Das M, Mahata SK, Mahata M, Wang L, Zhang K, Greenwood TA, Shih PA, Cockburn MG, Ziegler MG, Stridsberg M, Martin NG, Whitfield JB. Heritability and genome-wide linkage in us and australian twins identify novel genomic regions controlling chromogranin a: Implications for secretion and blood pressure. *Circulation*. 2008;118:247-257
19. O'Connor DT, Takiyyuddin MA, Printz MP, Dinh TQ, Barbosa JA, Rozansky DJ, Mahata SK, Wu H, Kennedy BP, Ziegler MG, Wright FA, Schlager G, Parmer RJ. Catecholamine storage vesicle protein expression in genetic hypertension. *Blood Press*. 1999;8:285-295
20. O'Connor DT, Kailasam MT, Kennedy BP, Ziegler MG, Yanaihara N, Parmer RJ. Early decline in the catecholamine release-inhibitory peptide catestatin in humans at genetic risk of hypertension. *J Hypertens*. 2002;20:1335-1345
21. Wen G, Mahata SK, Cadman P, Mahata M, Ghosh S, Mahapatra NR, Rao F, Stridsberg M, Smith DW, Mahboubi P, Schork NJ, O'Connor DT, Hamilton BA. Both rare and common polymorphisms contribute functional variation at chga, a regulator of catecholamine physiology. *Am J Hum Genet*. 2004;74:197-207
22. Rao F, Wen G, Gayen JR, Das M, Vaingankar SM, Rana BK, Mahata M, Kennedy BP, Salem RM, Stridsberg M, Abel K, Smith DW, Eskin E, Schork NJ, Hamilton BA, Ziegler MG, Mahata SK, O'Connor DT. Catecholamine release-inhibitory peptide catestatin (chromogranin a(352-372)): Naturally occurring amino acid variant gly364ser causes profound changes in human autonomic activity and alters risk for hypertension. *Circulation*. 2007;115:2271-2281
23. Biswas N, Vaingankar SM, Mahata M, Das M, Gayen JR, Taupenot L, Torpey JW, O'Connor DT, Mahata SK. Proteolytic cleavage of human chromogranin a containing naturally occurring catestatin variants: Differential processing at catestatin region by plasmin. *Endocrinology*. 2008;149:749-757
24. Angelone T, Quintieri AM, Brar BK, Limchaiyawat PT, Tota B, Mahata SK, Cerra MC. The antihypertensive chromogranin a peptide catestatin acts as a novel endocrine/paracrine modulator of cardiac inotropism and lusitropism. *Endocrinology*. 2008;149:4780-4793
25. Biswas N, Rodriguez-Flores JL, Courel M, Gayen JR, Vaingankar SM, Mahata M, Torpey JW, Taupenot L, O'Connor DT, Mahata SK. Cathepsin l co-localizes with chromogranin a in chromaffin vesicles to generate active peptides. *Endocrinology*. 2009;150:3547-3557
26. Sahu BS, Obbineni JM, Sahu G, Allu PK, Subramanian L, Sonawane PJ, Singh PK, Sasi BK, Senapati S, Maji SK, Bera AK, Gomathi BS, Mullasari AS, Mahapatra NR. Functional genetic variants of the catecholamine-release-inhibitory peptide catestatin in an indian population: Allele-specific effects on metabolic traits. *J Biol Chem*. 2012;287:43840-43852
27. Choi Y, Miura M, Nakata Y, Sugasawa T, Nissato S, Otsuki T, Sugawara J, Iemitsu M, Kawakami Y, Shimano H, Iijima Y, Tanaka K, Kuno S, Allu PK, Mahapatra NR, Maeda S, Takekoshi K. A common genetic variant of the chromogranin a-derived peptide catestatin is associated with atherogenesis and hypertension in a japanese population. *Endocr J*. 2015;62:797-804
28. Kiranmayi M, Chirasani VR, Allu PK, Subramanian L, Martelli EE, Sahu BS, Vishnuprabu D, Kumaragurubaran R, Sharma S, Bodhini D, Dixit M, Munirajan AK, Khullar M, Radha V, Mohan V, Mullasari AS, Naga Prasad SV, Senapati S, Mahapatra NR. Catestatin

882 gly364ser variant alters systemic blood pressure and the risk for hypertension in human
883 populations via endothelial nitric oxide pathway. *Hypertension*. 2016
884 29. Ottesen AH, Carlson CR, Louch WE, Dahl MB, Sandbu RA, Johansen RF, Jarstadmarken
885 H, Bjoras M, Hoiseth AD, Brynildsen J, Sjaastad I, Stridsberg M, Omland T, Christensen
886 G, Rosjo H. Glycosylated chromogranin a in heart failure: Implications for processing and
887 cardiomyocyte calcium homeostasis. *Circ Heart Fail*. 2017;10
888 30. Mahapatra NR, O'Connor DT, Vaingankar SM, Hikim AP, Mahata M, Ray S, Staite E, Wu
889 H, Gu Y, Dalton N, Kennedy BP, Ziegler MG, Ross J, Mahata SK. Hypertension from
890 targeted ablation of chromogranin a can be rescued by the human ortholog. *J Clin Invest*.
891 2005;115:1942-1952
892 31. Bandyopadhyay GK, Vu CU, Gentile S, Lee H, Biswas N, Chi NW, O'Connor DT, Mahata
893 SK. Catestatin (chromogranin a(352-372)) and novel effects on mobilization of fat from
894 adipose tissue through regulation of adrenergic and leptin signaling. *J Biol Chem*.
895 2012;287:23141-23151
896 32. Ratti S, Curnis F, Longhi R, Colombo B, Gasparri A, Magni F, Manera E, Metz-Boutigue
897 MH, Corti A. Structure-activity relationships of chromogranin a in cell adhesion.
898 Identification of an adhesion site for fibroblasts and smooth muscle cells [in process
899 citation]. *J Biol Chem*. 2000;275:29257-29263
900 33. Bianco M, Gasparri AM, Colombo B, Curnis F, Girlanda S, Ponzoni M, Bertilaccio MT,
901 Calcinotto A, Sacchi A, Ferrero E, Ferrarini M, Chesi M, Bergsagel PL, Bellone M, Tonon
902 G, Ciceri F, Marcatti M, Caligaris-Cappio F, Corti A. Chromogranin a is preferentially
903 cleaved into proangiogenic peptides in the bone marrow of multiple myeloma patients.
904 *Cancer Res*. 2016;76:1781-1791
905 34. Hulsmans M, Sager HB, Roh JD, Valero-Munoz M, Houstis NE, Iwamoto Y, Sun Y, Wilson
906 RM, Wojtkiewicz G, Tricot B, Osborne MT, Hung J, Vinegoni C, Naxerova K, Sosnovik
907 DE, Zile MR, Bradshaw AD, Liao R, Tawakol A, Weissleder R, Rosenzweig A, Swirski FK,
908 Sam F, Nahrendorf M. Cardiac macrophages promote diastolic dysfunction. *J Exp Med*.
909 2018;215:423-440
910 35. Pasqua T, Mahata S, Bandyopadhyay GK, Biswas A, Perkins GA, Sinha-Hikim AP,
911 Goldstein DS, Eiden LE, Mahata SK. Impact of chromogranin a deficiency on
912 catecholamine storage, catecholamine granule morphology and chromaffin cell energy
913 metabolism in vivo. *Cell Tissue Res*. 2016;363:693-712
914 36. Hsiao A, Worrall DS, Olefsky JM, Subramaniam S. Variance-modeled posterior inference
915 of microarray data: Detecting gene-expression changes in 3t3-l1 adipocytes.
916 *Bioinformatics*. 2004;20:3108-3127
917 37. Bligh EG, Dyer WJ. A rapid method of total lipid extraction and purification. *Can J Biochem*
918 *Physiol*. 1959;37:911-917
919 38. Folch J, Lees M, Sloane Stanley GH. A simple method for the isolation and purification of
920 total lipides from animal tissues. *J Biol Chem*. 1957;226:497-509
921 39. Tang K, Pasqua T, Biswas A, Mahata S, Tang J, Tang A, Bandyopadhyay GK, Sinha-
922 Hikim AP, Chi NW, Webster NJ, Corti A, Mahata SK. Muscle injury, impaired muscle
923 function and insulin resistance in chromogranin a-knockout mice. *J Endocrinol*.
924 2017;232:137-153
925 40. Carroll NV, Longley RW, Roe JH. The determination of glycogen in liver and muscle by
926 use of anthrone reagent. *J Biol Chem*. 1956;220:583-593
927 41. Headrick JP, Willems L, Ashton KJ, Holmgren K, Peart J, Matherne GP. Ischaemic
928 tolerance in aged mouse myocardium: The role of adenosine and effects of a1 adenosine
929 receptor overexpression. *J Physiol*. 2003;549:823-833
930 42. Ying W, Mahata S, Bandyopadhyay GK, Zhou Z, Wollam J, Vu J, Mayoral R, Chi NW,
931 Webster NJG, Corti A, Mahata SK. Catestatin inhibits obesity-induced macrophage

932 infiltration and inflammation in the liver and suppresses hepatic glucose production,
933 leading to improved insulin sensitivity. *Diabetes*. 2018;67:841-848
934 43. Kojima M, Ozawa N, Mori Y, Takahashi Y, Watanabe-Kominato K, Shirai R, Watanabe R,
935 Sato K, Matsuyama TA, Ishibashi-Ueda H, Koba S, Kobayashi Y, Hirano T, Watanabe T.
936 Catestatin prevents macrophage-driven atherosclerosis but not arterial injury-induced
937 neointimal hyperplasia. *Thromb Haemost*. 2018;118:182-194
938 44. Chen H, Liu D, Ge L, Wang T, Ma Z, Han Y, Duan Y, Xu X, Liu W, Yuan J, Liu J, Li R, Du
939 R. Catestatin prevents endothelial inflammation and promotes thrombus resolution in
940 acute pulmonary embolism in mice. *Biosci Rep*. 2019;39
941 45. Zivkovic PM, Matetic A, Tadin Hadjina I, Rusic D, Vilovic M, Supe-Domic D, Borovac JA,
942 Mudnic I, Tonkic A, Bozic J. Serum catestatin levels and arterial stiffness parameters are
943 increased in patients with inflammatory bowel disease. *J Clin Med*. 2020;9
944 46. Avolio E, Mahata SK, Mantuano E, Mele M, Alo R, Facciolo RM, Talani G, Canonaco M.
945 Antihypertensive and neuroprotective effects of catestatin in spontaneously hypertensive
946 rats: Interaction with gabaergic transmission in amygdala and brainstem. *Neuroscience*.
947 2014;270:48-57
948 47. Granger JP. An emerging role for inflammatory cytokines in hypertension. *Am J Physiol*
949 *Heart Circ Physiol*. 2006;290:H923-924
950 48. Lee DL, Sturgis LC, Labazi H, Osborne JB, Jr., Fleming C, Pollock JS, Manhiani M, Imig
951 JD, Brands MW. Angiotensin ii hypertension is attenuated in interleukin-6 knockout mice.
952 *Am J Physiol Heart Circ Physiol*. 2006;290:H935-940
953 49. Brands MW, Banes-Berceli AK, Inscho EW, Al-Azawi H, Allen AJ, Labazi H. Interleukin 6
954 knockout prevents angiotensin ii hypertension: Role of renal vasoconstriction and janus
955 kinase 2/signal transducer and activator of transcription 3 activation. *Hypertension*.
956 2010;56:879-884
957 50. Lima VV, Zemse SM, Chiao CW, Bomfim GF, Tostes RC, Clinton Webb R, Giachini FR.
958 Interleukin-10 limits increased blood pressure and vascular rhoa/rho-kinase signaling in
959 angiotensin ii-infused mice. *Life Sci*. 2016;145:137-143
960 51. Ishimitsu T, Uehara Y, Numabe A, Tsukada H, Ogawa Y, Yagi S. Antihypertensive effect
961 of interleukin-2 in salt-sensitive dahl rats. *Hypertension*. 1994;23:68-73
962 52. Tuttle RS, Boppana DP. Antihypertensive effect of interleukin-2. *Hypertension*.
963 1990;15:89-94
964 53. Tinsley JH, South S, Chiasson VL, Mitchell BM. Interleukin-10 reduces inflammation,
965 endothelial dysfunction, and blood pressure in hypertensive pregnant rats. *Am J Physiol*
966 *Regul Integr Comp Physiol*. 2010;298:R713-719
967 54. Viel EC, Lemarie CA, Benkirane K, Paradis P, Schiffrin EL. Immune regulation and
968 vascular inflammation in genetic hypertension. *Am J Physiol Heart Circ Physiol*.
969 2010;298:H938-944
970 55. Ritterhoff J, Tian R. Metabolism in cardiomyopathy: Every substrate matters. *Cardiovasc*
971 *Res*. 2017;113:411-421
972 56. Lopaschuk GD, Belke DD, Gamble J, Itoi T, Schonekess BO. Regulation of fatty acid
973 oxidation in the mammalian heart in health and disease. *Biochim Biophys Acta*.
974 1994;1213:263-276
975 57. Stanley WC, Lopaschuk GD, Hall JL, McCormack JG. Regulation of myocardial
976 carbohydrate metabolism under normal and ischaemic conditions. Potential for
977 pharmacological interventions. *Cardiovasc Res*. 1997;33:243-257
978 58. Mishra PK, Ying W, Nandi SS, Bandyopadhyay GK, Patel KK, Mahata SK. Diabetic
979 cardiomyopathy: An immunometabolic perspective. *Front Endocrinol (Lausanne)*.
980 2017;8:72
981 59. Sokolowska E, Blachnio-Zabielska A. The role of ceramides in insulin resistance. *Front*
982 *Endocrinol (Lausanne)*. 2019;10:577

983 60. Dasgupta A, Bandyopadhyay GK, Ray I, Bandyopadhyay K, Chowdhury N, De RK,
984 Mahata SK. Catestatin improves insulin sensitivity by attenuating endoplasmic reticulum
985 stress: In vivo and in silico validation. *Comput Struct Biotechnol J*. 2020;18:464-481
986 61. Mehta MM, Weinberg SE, Chandel NS. Mitochondrial control of immunity: Beyond atp.
987 *Nat Rev Immunol*. 2017;17:608-620
988 62. Touyz RM. Reactive oxygen species, vascular oxidative stress, and redox signaling in
989 hypertension: What is the clinical significance? *Hypertension*. 2004;44:248-252
990 63. Cogliati S, Frezza C, Soriano ME, Varanita T, Quintana-Cabrera R, Corrado M, Cipolat S,
991 Costa V, Casarin A, Gomes LC, Perales-Clemente E, Salviati L, Fernandez-Silva P,
992 Enriquez JA, Scorrano L. Mitochondrial cristae shape determines respiratory chain
993 supercomplexes assembly and respiratory efficiency. *Cell*. 2013;155:160-171
994 64. Hollander JM, Thapa D, Shepherd DL. Physiological and structural differences in spatially
995 distinct subpopulations of cardiac mitochondria: Influence of cardiac pathologies. *Am J*
996 *Physiol Heart Circ Physiol*. 2014;307:H1-14
997 65. Crochemore C, Mekki M, Corbiere C, Karoui A, Noel R, Vendeville C, Vaugeois JM,
998 Monteil C. Subsarcolemmal and interfibrillar mitochondria display distinct superoxide
999 production profiles. *Free Radic Res*. 2015;49:331-337
1000 66. How OJ, Aasum E, Severson DL, Chan WY, Essop MF, Larsen TS. Increased myocardial
1001 oxygen consumption reduces cardiac efficiency in diabetic mice. *Diabetes*. 2006;55:466-
1002 473
1003 67. Westermeier F, Navarro-Marquez M, Lopez-Crisosto C, Bravo-Sagua R, Quiroga C,
1004 Bustamante M, Verdejo HE, Zalaquett R, Ibacache M, Parra V, Castro PF, Rothermel BA,
1005 Hill JA, Lavandero S. Defective insulin signaling and mitochondrial dynamics in diabetic
1006 cardiomyopathy. *Biochim Biophys Acta*. 2015;1853:1113-1118
1007 68. Gomes LC, Di Benedetto G, Scorrano L. During autophagy mitochondria elongate, are
1008 spared from degradation and sustain cell viability. *Nat Cell Biol*. 2011;13:589-598
1009 69. Green DR, Galluzzi L, Kroemer G. Mitochondria and the autophagy-inflammation-cell
1010 death axis in organismal aging. *Science*. 2011;333:1109-1112
1011 70. Delbridge LMD, Mellor KM, Taylor DJ, Gottlieb RA. Myocardial stress and autophagy:
1012 Mechanisms and potential therapies. *Nat Rev Cardiol*. 2017;14:412-425
1013 71. Pende A, Musso NR, Vergassola C, Puppo F, Ioverno A, Criscuolo D, Indiveri F, Lotti G.
1014 Neuroendocrine effects of interferon alpha 2-a in healthy human subjects. *J Biol Regul*
1015 *Homeost Agents*. 1990;4:67-72
1016 72. Corssmit EP, Heijligenberg R, Endert E, Ackermans MT, Sauerwein HP, Romijn JA.
1017 Endocrine and metabolic effects of interferon-alpha in humans. *J Clin Endocrinol Metab*.
1018 1996;81:3265-3269
1019 73. Kannan H, Tanaka Y, Kunitake T, Ueta Y, Hayashida Y, Yamashita H. Activation of
1020 sympathetic outflow by recombinant human interleukin-1 beta in conscious rats. *Am J*
1021 *Physiol*. 1996;270:R479-485
1022 74. Rivier C, Vale W, Brown M. In the rat, interleukin-1 alpha and -beta stimulate
1023 adrenocorticotropin and catecholamine release. *Endocrinology*. 1989;125:3096-3102
1024 75. Darling G, Goldstein DS, Stull R, Gorschboth CM, Norton JA. Tumor necrosis factor:
1025 Immune endocrine interaction. *Surgery*. 1989;106:1155-1160
1026 76. De Laurentiis A, Pisera D, Caruso C, Candolfi M, Mohn C, Rettori V, Seilicovich A.
1027 Lipopolysaccharide- and tumor necrosis factor-alpha-induced changes in prolactin
1028 secretion and dopaminergic activity in the hypothalamic-pituitary axis.
1029 *Neuroimmunomodulation*. 2002;10:30-39
1030 77. Epelman S, Lavine KJ, Beaudin AE, Sojka DK, Carrero JA, Calderon B, Brija T, Gautier
1031 EL, Ivanov S, Satpathy AT, Schilling JD, Schwendener R, Sergin I, Razani B, Forsberg
1032 EC, Yokoyama WM, Unanue ER, Colonna M, Randolph GJ, Mann DL. Embryonic and

adult-derived resident cardiac macrophages are maintained through distinct mechanisms at steady state and during inflammation. *Immunity*. 2014;40:91-104

78. Lavine KJ, Epelman S, Uchida K, Weber KJ, Nichols CG, Schilling JD, Ornitz DM, Randolph GJ, Mann DL. Distinct macrophage lineages contribute to disparate patterns of cardiac recovery and remodeling in the neonatal and adult heart. *Proc Natl Acad Sci U S A*. 2014;111:16029-16034
79. Leid J, Carrelha J, Boukarabila H, Epelman S, Jacobsen SE, Lavine KJ. Primitive embryonic macrophages are required for coronary development and maturation. *Circ Res*. 2016;118:1498-1511
80. Heo GS, Kopecky B, Sultan D, Ou M, Feng G, Bajpai G, Zhang X, Luehmann H, Detering L, Su Y, Leuschner F, Combadiere C, Kreisel D, Gropler RJ, Brody SL, Liu Y, Lavine KJ. Molecular imaging visualizes recruitment of inflammatory monocytes and macrophages to the injured heart. *Circ Res*. 2019;124:881-890
81. Bajpai G, Schneider C, Wong N, Bredemeyer A, Hulsmans M, Nahrendorf M, Epelman S, Kreisel D, Liu Y, Itoh A, Shankar TS, Selzman CH, Drakos SG, Lavine KJ. The human heart contains distinct macrophage subsets with divergent origins and functions. *Nat Med*. 2018;24:1234-1245
82. Bajpai G, Bredemeyer A, Li W, Zaitsev K, Koenig AL, Lokshina I, Mohan J, Ivey B, Hsiao HM, Weinheimer C, Kovacs A, Epelman S, Artyomov M, Kreisel D, Lavine KJ. Tissue resident ccr2- and ccr2+ cardiac macrophages differentially orchestrate monocyte recruitment and fate specification following myocardial injury. *Circ Res*. 2019;124:263-278
83. Heidt T, Courties G, Dutta P, Sager HB, Sebas M, Iwamoto Y, Sun Y, Da Silva N, Panizzi P, van der Laan AM, Swirski FK, Weissleder R, Nahrendorf M. Differential contribution of monocytes to heart macrophages in steady-state and after myocardial infarction. *Circ Res*. 2014;115:284-295
84. Mann DL. Innate immunity and the failing heart: The cytokine hypothesis revisited. *Circ Res*. 2015;116:1254-1268
85. Dick SA, Epelman S. Chronic heart failure and inflammation: What do we really know? *Circ Res*. 2016;119:159-176
86. Bergman MR, Kao RH, McCune SA, Holycross BJ. Myocardial tumor necrosis factor-alpha secretion in hypertensive and heart failure-prone rats. *Am J Physiol*. 1999;277:H543-550
87. Levine B, Kalman J, Mayer L, Fillit HM, Packer M. Elevated circulating levels of tumor necrosis factor in severe chronic heart failure. *N Engl J Med*. 1990;323:236-241
88. Kubota T, McTiernan CF, Frye CS, Slawson SE, Lemster BH, Koretsky AP, Demetris AJ, Feldman AM. Dilated cardiomyopathy in transgenic mice with cardiac-specific overexpression of tumor necrosis factor-alpha. *Circ Res*. 1997;81:627-635
89. Ashrafian H, Frenneaux MP, Opie LH. Metabolic mechanisms in heart failure. *Circulation*. 2007;116:434-448
90. Mootha VK, Arai AE, Balaban RS. Maximum oxidative phosphorylation capacity of the mammalian heart. *Am J Physiol*. 1997;272:H769-775
91. Balaban RS. Cardiac energy metabolism homeostasis: Role of cytosolic calcium. *J Mol Cell Cardiol*. 2002;34:1259-1271
92. Neubauer S. The failing heart--an engine out of fuel. *N Engl J Med*. 2007;356:1140-1151
93. Hall CJ, Sanderson LE, Crosier KE, Crosier PS. Mitochondrial metabolism, reactive oxygen species, and macrophage function-fishing for insights. *J Mol Med (Berl)*. 2014;92:1119-1128
94. Ingwall JS. Energy metabolism in heart failure and remodelling. *Cardiovasc Res*. 2009;81:412-419
95. Neely JR, Rovetto MJ, Oram JF. Myocardial utilization of carbohydrate and lipids. *Prog Cardiovasc Dis*. 1972;15:289-329

1083 96. Taegtmeyer H, Golfman L, Sharma S, Razeghi P, van Arsdall M. Linking gene expression
1084 to function: Metabolic flexibility in the normal and diseased heart. *Ann N Y Acad Sci*.
1085 2004;1015:202-213
1086 97. Marelli-Berg FM, Aksentijevic D. Immunometabolic cross-talk in the inflamed heart. *Cell*
1087 *Stress*. 2019;3:240-266
1088 98. Stanley WC, Recchia FA, Lopaschuk GD. Myocardial substrate metabolism in the normal
1089 and failing heart. *Physiol Rev*. 2005;85:1093-1129
1090 99. Bertero E, Maack C. Metabolic remodelling in heart failure. *Nat Rev Cardiol*. 2018;15:457-
1091 470
1092 100. Buchanan J, Mazumder PK, Hu P, Chakrabarti G, Roberts MW, Yun UJ, Cooksey RC,
1093 Litwin SE, Abel ED. Reduced cardiac efficiency and altered substrate metabolism
1094 precedes the onset of hyperglycemia and contractile dysfunction in two mouse models of
1095 insulin resistance and obesity. *Endocrinology*. 2005;146:5341-5349
1096 101. Mazumder PK, O'Neill BT, Roberts MW, Buchanan J, Yun UJ, Cooksey RC, Boudina S,
1097 Abel ED. Impaired cardiac efficiency and increased fatty acid oxidation in insulin-resistant
1098 ob/ob mouse hearts. *Diabetes*. 2004;53:2366-2374
1099 102. Wang P, Lloyd SG, Zeng H, Bonen A, Chatham JC. Impact of altered substrate utilization
1100 on cardiac function in isolated hearts from zucker diabetic fatty rats. *Am J Physiol Heart*
1101 *Circ Physiol*. 2005;288:H2102-2110
1102 103. Lopaschuk GD, Folmes CD, Stanley WC. Cardiac energy metabolism in obesity. *Circ Res*.
1103 2007;101:335-347
1104 104. Fukushima A, Lopaschuk GD. Cardiac fatty acid oxidation in heart failure associated with
1105 obesity and diabetes. *Biochim Biophys Acta*. 2016;1861:1525-1534
1106 105. Chess DJ, Stanley WC. Role of diet and fuel overabundance in the development and
1107 progression of heart failure. *Cardiovasc Res*. 2008;79:269-278
1108 106. Rimbaud S, Ruiz M, Piquereau J, Mateo P, Fortin D, Veksler V, Garnier A, Ventura-Clapier
1109 R. Resveratrol improves survival, hemodynamics and energetics in a rat model of
1110 hypertension leading to heart failure. *PLoS One*. 2011;6:e26391
1111 107. Lopaschuk GD, Ussher JR, Folmes CD, Jaswal JS, Stanley WC. Myocardial fatty acid
1112 metabolism in health and disease. *Physiol Rev*. 2010;90:207-258
1113 108. Zlobine I, Gopal K, Ussher JR. Lipotoxicity in obesity and diabetes-related cardiac
1114 dysfunction. *Biochim Biophys Acta*. 2016;1861:1555-1568
1115 109. Nakanishi T, Kato S. Impact of diabetes mellitus on myocardial lipid deposition: An
1116 autopsy study. *Pathol Res Pract*. 2014;210:1018-1025
1117 110. D'Souza K, Nzirorera C, Kienesberger PC. Lipid metabolism and signaling in cardiac
1118 lipotoxicity. *Biochim Biophys Acta*. 2016;1861:1513-1524
1119 111. Unger RH. Lipotoxic diseases. *Annu Rev Med*. 2002;53:319-336
1120 112. Peterson LR, Herrero P, Schechtman KB, Racette SB, Waggoner AD, Kisrieva-Ware Z,
1121 Dence C, Klein S, Marsala J, Meyer T, Gropler RJ. Effect of obesity and insulin resistance
1122 on myocardial substrate metabolism and efficiency in young women. *Circulation*.
1123 2004;109:2191-2196
1124 113. Gray S, Kim JK. New insights into insulin resistance in the diabetic heart. *Trends in*
1125 *endocrinology and metabolism: TEM*. 2011;22:394-403
1126 114. Rider OJ, Lewis AJ, Neubauer S. Structural and metabolic effects of obesity on the
1127 myocardium and the aorta. *Obes Facts*. 2014;7:329-338
1128 115. Smith EL, Schuchman EH. The unexpected role of acid sphingomyelinase in cell death
1129 and the pathophysiology of common diseases. *FASEB J*. 2008;22:3419-3431
1130 116. Anderson EA, Sinkey CA, Lawton WJ, Mark AL. Elevated sympathetic nerve activity in
1131 borderline hypertensive humans. Evidence from direct intraneural recordings.
1132 *Hypertension*. 1989;14:177-183

1133 117. Smith PA, Graham LN, Mackintosh AF, Stoker JB, Mary DA. Relationship between central
1134 sympathetic activity and stages of human hypertension. *Am J Hypertens*. 2004;17:217-
1135 222
1136 118. Grassi G, Cattaneo BM, Seravalle G, Lanfranchi A, Mancia G. Baroreflex control of
1137 sympathetic nerve activity in essential and secondary hypertension. *Hypertension*.
1138 1998;31:68-72
1139 119. Grassi G. Role of the sympathetic nervous system in human hypertension. *J Hypertens*.
1140 1998;16:1979-1987
1141 120. Judy WV, Farrell SK. Arterial baroreceptor reflex control of sympathetic nerve activity in
1142 the spontaneously hypertensive rat. *Hypertension*. 1979;1:605-614
1143 121. Lundin S, Ricksten SE, Thoren P. Renal sympathetic activity in spontaneously
1144 hypertensive rats and normotensive controls, as studied by three different methods. *Acta*
1145 *Physiol Scand*. 1984;120:265-272
1146 122. Elenkov IJ, Wilder RL, Chrousos GP, Vizi ES. The sympathetic nerve--an integrative
1147 interface between two supersystems: The brain and the immune system. *Pharmacol Rev*.
1148 2000;52:595-638
1149 123. Libby P, Ridker PM, Maseri A. Inflammation and atherosclerosis. *Circulation*.
1150 2002;105:1135-1143
1151 124. Mahata SK, Mahata M, Wakade AR, O'Connor DT. Primary structure and function of the
1152 catecholamine release inhibitory peptide catestatin (chromogranin a344-364):
1153 Identification of amino acid residues crucial for activity. *Mol Endocrinol*. 2000;14:1525-
1154 1535
1155 125. Mahata SK, Mahapatra NR, Mahata M, Wang TC, Kennedy BP, Ziegler MG, O'Connor
1156 DT. Catecholamine secretory vesicle stimulus-transcription coupling in vivo.
1157 Demonstration by a novel transgenic promoter/photoprotein reporter and inhibition of
1158 secretion and transcription by the chromogranin a fragment catestatin. *J Biol Chem*.
1159 2003;278:32058-32067
1160

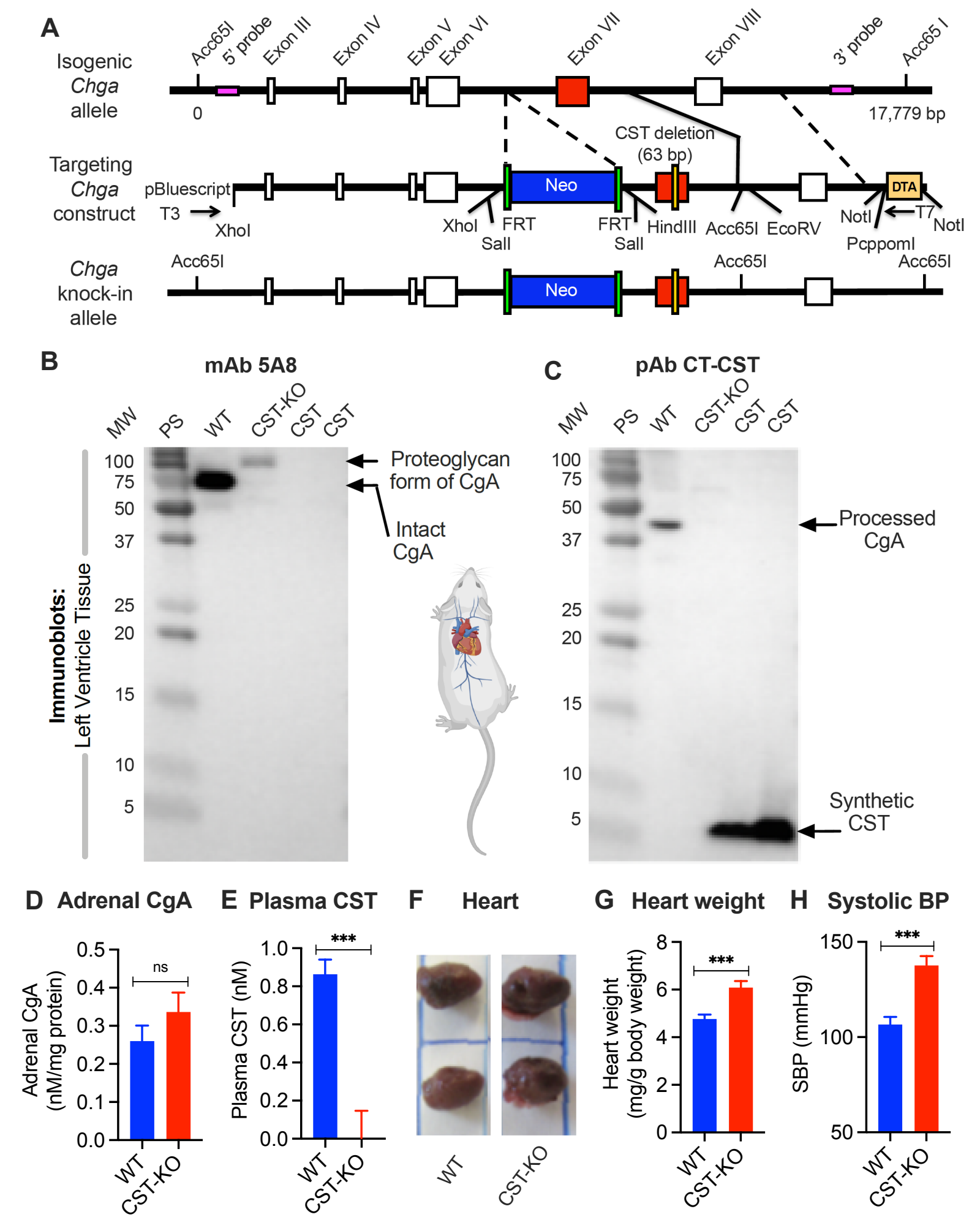
A
Isogenic Chga allele
Acc65I
5' probe
Exon III
Exon IV
Exon V
Exon VI
Exon VII
Exon VIII
3' probe
Acc65 I
0
17,779 bp
CST deletion (63 bp)
Targeting Chga construct
pBluescript
T3
XhoI
Neo
XhoI
FRT
SalI
FRT
SalI
HindIII
Acc65I
EcoRV
DTA
NotI
T7
NotI
PcppomI
Chga knock-in allele
Acc65I
Neo
Acc65I
Acc65I
B
mAb 5A8
MW
PS
WT
CST-KO
CST
CST
100
75
50
37
25
20
15
10
5
Proteoglycan form of CgA
Intact CgA
Immunoblots:
Left Ventricle Tissue
C
pAb CT-CST
MW
PS
WT
CST-KO
CST
CST
Processed CgA
Synthetic CST
D Adrenal CgA
Adrenal CgA (nM/mg protein)
ns
WT
CST-KO
E Plasma CST
Plasma CST (nM)
***
WT
CST-KO
F Heart
WT
CST-KO
G Heart weight
Heart weight (mg/g body weight)
***
WT
CST-KO
H Systolic BP
SBP (mmHg)
***
WT
CST-KO

Fig. 1

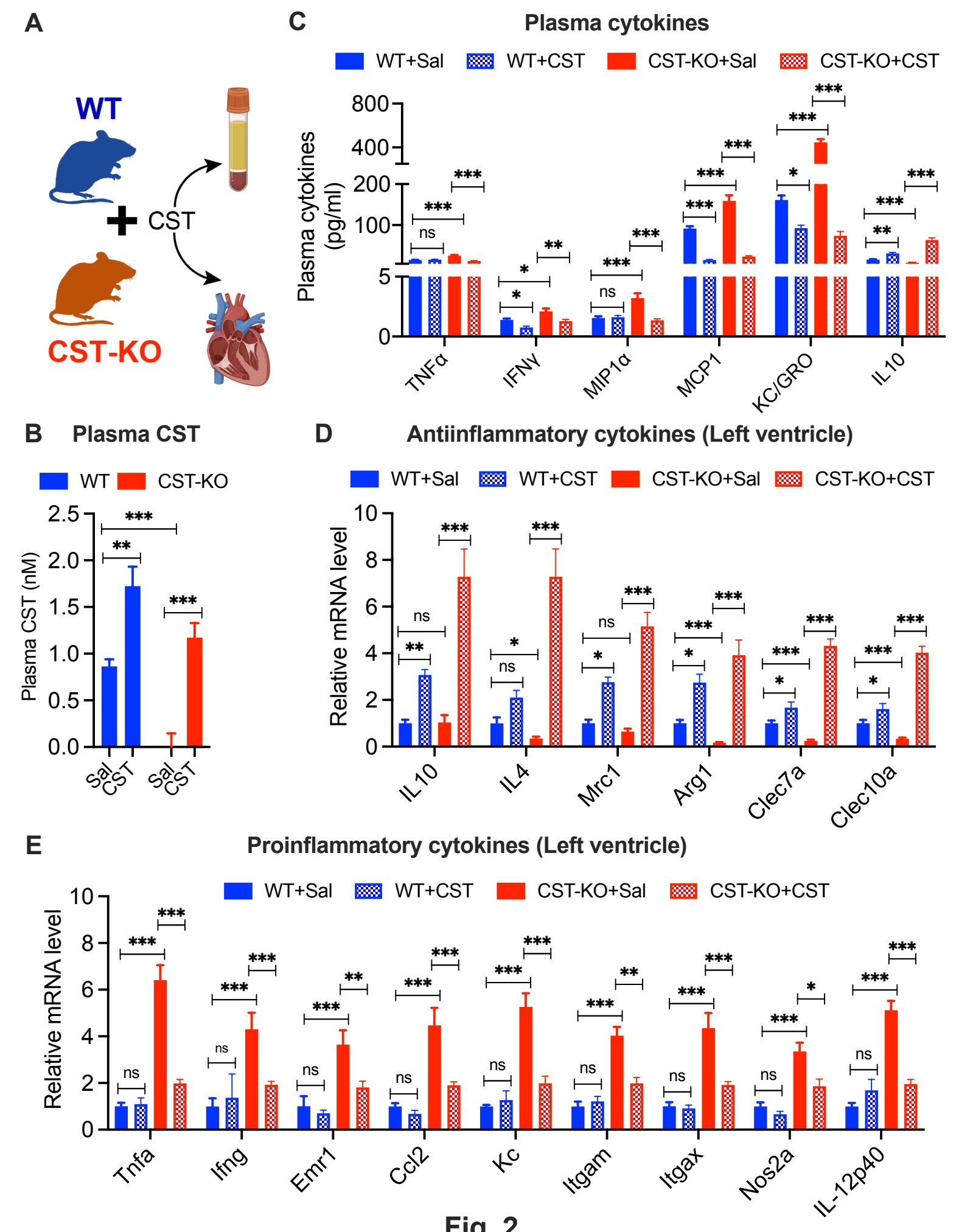
A
WT
CST
CST-KO
B
Plasma CST
WT
CST-KO
Plasma CST (nM)
Sal
CST
Sal
CST
C
Plasma cytokines
WT+Sal
WT+CST
CST-KO+Sal
CST-KO+CST
Plasma cytokines (pg/ml)
TNFα
IFNγ
MIP1α
MCP1
KC/GRO
IL10
D
Antiinflammatory cytokines (Left ventricle)
Relative mRNA level
IL10
IL4
Mrc1
Arg1
Clec7a
Clec10a
E
Proinflammatory cytokines (Left ventricle)
Relative mRNA level
Tnfa
Ifng
Emr1
Ccl2
Kc
Itgam
Itgax
Nos2a
IL-12p40

Fig. 2

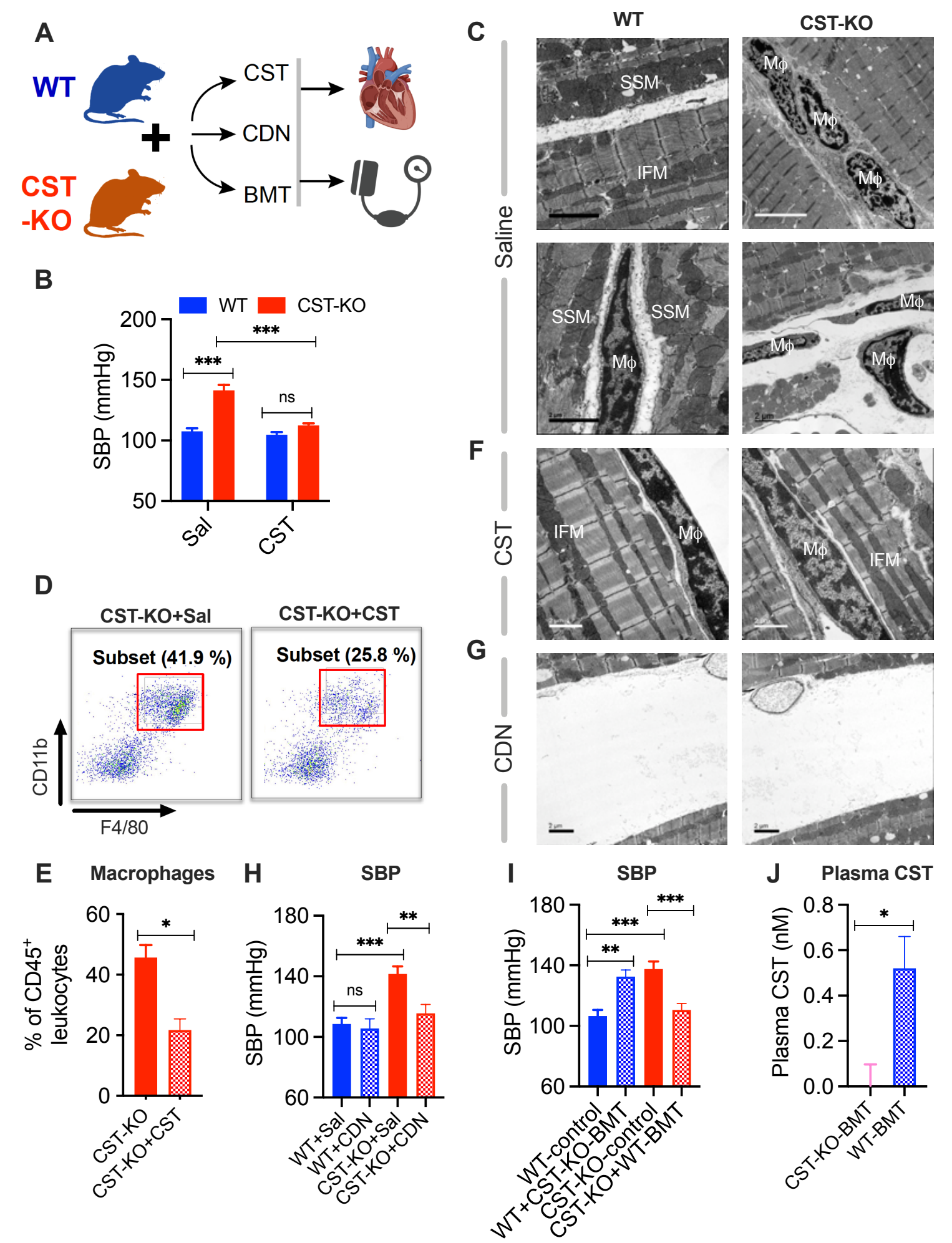
A
WT
CST
-KO
CST
CDN
BMT
B
WT
CST-KO
SBP (mmHg)
200
150
100
50
***
***
ns
Sal
CST
C
WT
CST-KO
Saline
SSM
IFM
Mϕ
F
CST
G
CDN
D
CST-KO+Sal
CST-KO+CST
Subset (41.9 %)
Subset (25.8 %)
CD11b
F4/80
E
Macrophages
% of CD45+ leukocytes
60
40
20
0
*
CST-KO
CST-KO+CST
H
SBP
SBP (mmHg)
180
140
100
60
**
***
ns
WT+Sal
WT+CDN
CST-KO+Sal
CST-KO+CDN
I
SBP
SBP (mmHg)
180
140
100
60
***
***
**
WT-control
WT+CST-KO-BMT
CST-KO-control
CST-KO+WT-BMT
J
Plasma CST
Plasma CST (nM)
0.8
0.6
0.4
0.2
0.0
*
CST-KO-BMT
WT-BMT

Fig. 3

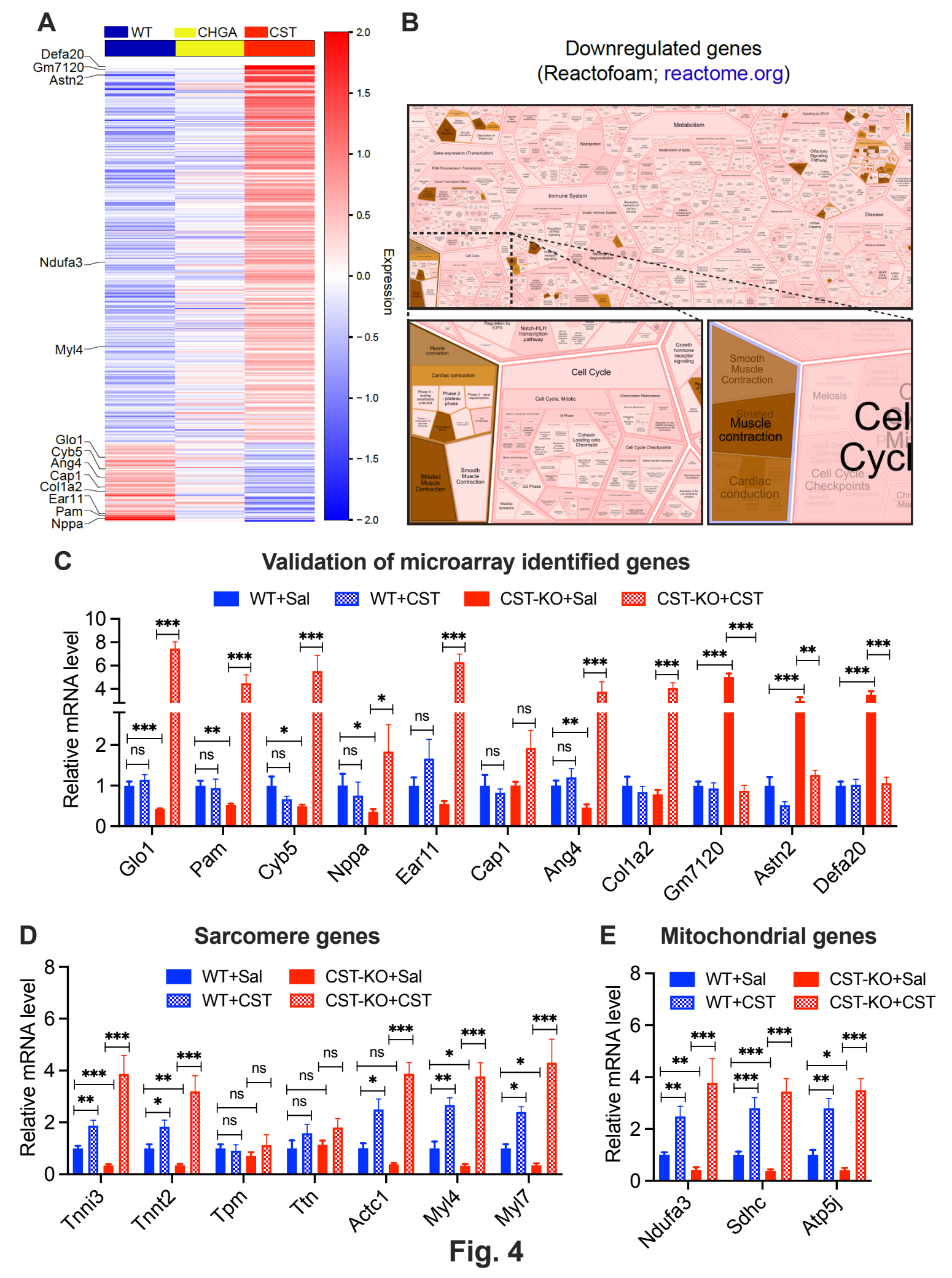
A
WT
CHGA
CST
Defa20
Gm7120
Astn2
Ndufa3
Myl4
Glo1
Cyb5
Ang4
Cap1
Col1a2
Ear11
Pam
Nppa
Expression
2.0
1.5
1.0
0.5
0.0
−0.5
−1.0
−1.5
−2.0
B
Downregulated genes
(Reactofoam; reactome.org)
Metabolism
Immune System
Disease
Cell Cycle
Cell Cycle, Mitotic
Cell Cycle Checkpoints
Cohesin Loading onto Chromatin
Notch-HLH transcription pathway
Growth hormone receptor signaling
Muscle contraction
Cardiac conduction
Striated Muscle Contraction
Smooth Muscle Contraction
Meiosis
C
Validation of microarray identified genes
WT+Sal
WT+CST
CST-KO+Sal
CST-KO+CST
Relative mRNA level
Glo1
Pam
Cyb5
Nppa
Ear11
Cap1
Ang4
Col1a2
Gm7120
Astn2
Defa20
D
Sarcomere genes
Tnni3
Tnnt2
Tpm
Ttn
Actc1
Myl4
Myl7
E
Mitochondrial genes
Ndufa3
Sdhc
Atp5j

Fig. 4

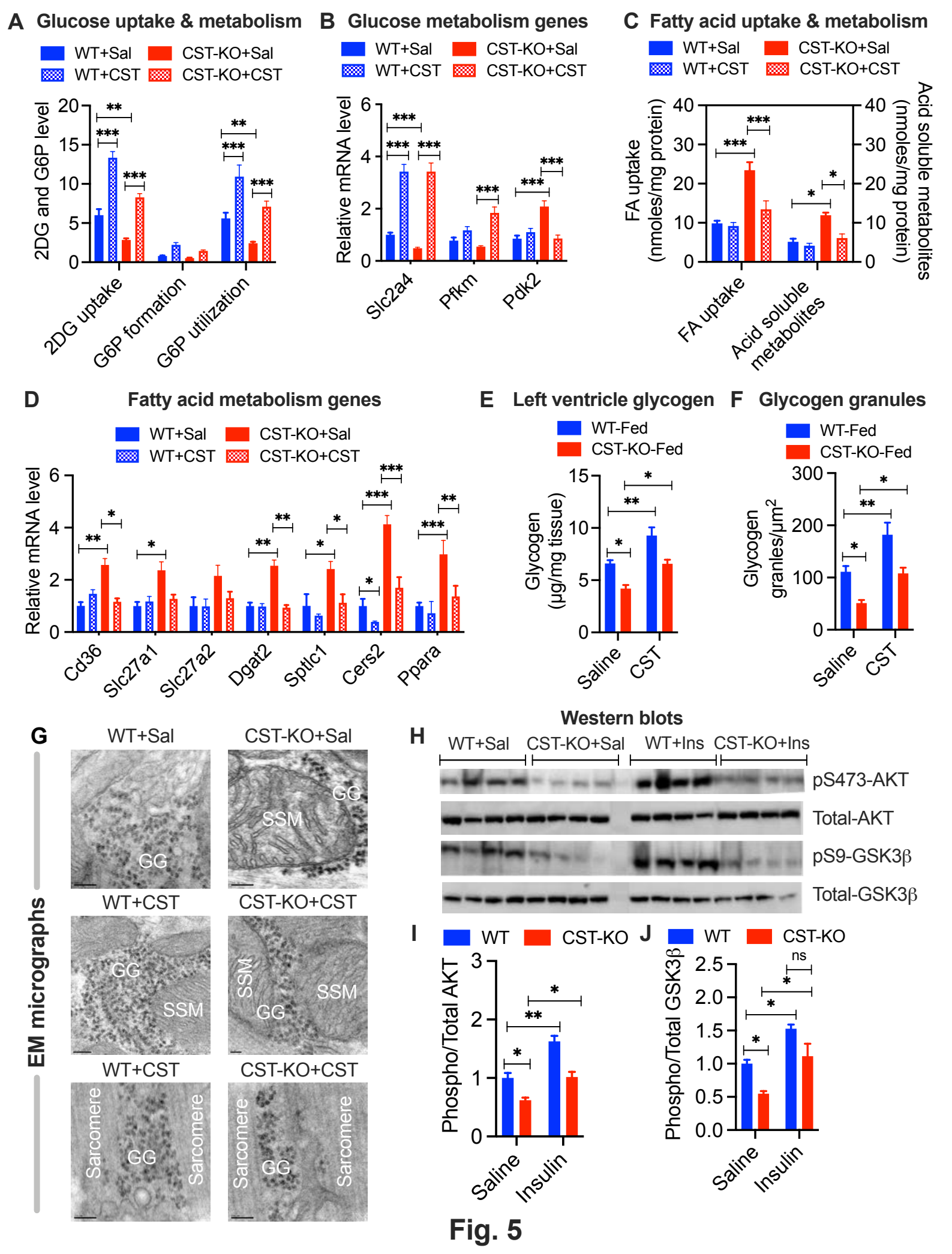
A Glucose uptake & metabolism
WT+Sal
CST-KO+Sal
WT+CST
CST-KO+CST
2DG and G6P level
2DG uptake
G6P formation
G6P utilization
B Glucose metabolism genes
Relative mRNA level
Slc2a4
Pfkm
Pdk2
C Fatty acid uptake & metabolism
FA uptake (nmoles/mg protein)
Acid soluble metabolites (nmoles/mg protein)
FA uptake
Acid soluble metabolites
D Fatty acid metabolism genes
Cd36
Slc27a1
Slc27a2
Dgat2
Sptlc1
Cers2
Ppara
E Left ventricle glycogen
WT-Fed
CST-KO-Fed
Glycogen (μg/mg tissue)
Saline
CST
F Glycogen granules
Glycogen granles/μm2
G
WT+Sal
CST-KO+Sal
WT+CST
CST-KO+CST
EM micrographs
GG
SSM
Sarcomere
H Western blots
WT+Sal
CST-KO+Sal
WT+Ins
CST-KO+Ins
pS473-AKT
Total-AKT
pS9-GSK3β
Total-GSK3β
I
WT
CST-KO
Phospho/Total AKT
Saline
Insulin
J
Phospho/Total GSK3β
ns

Fig. 5

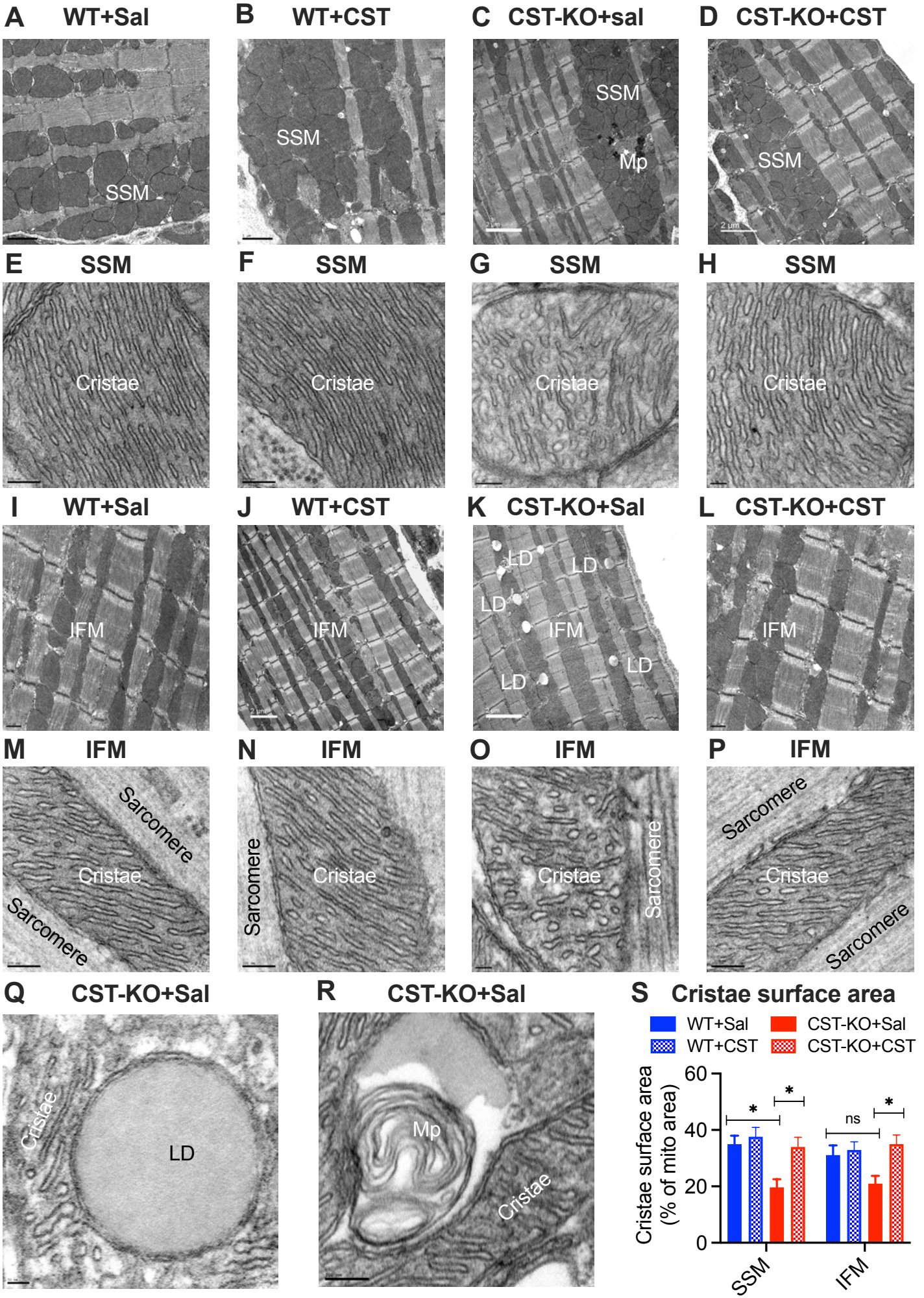
A WT+Sal
SSM
B WT+CST
SSM
C CST-KO+sal
SSM
Mp
D CST-KO+CST
SSM
E SSM
Cristae
F SSM
Cristae
G SSM
Cristae
H SSM
Cristae
I WT+Sal
IFM
J WT+CST
IFM
K CST-KO+Sal
LD
LD
LD
IFM
LD
LD
L CST-KO+CST
IFM
M IFM
Sarcomere
Cristae
Sarcomere
N IFM
Sarcomere
Cristae
O IFM
Cristae
Sarcomere
P IFM
Sarcomere
Cristae
Sarcomere
Q CST-KO+Sal
Cristae
LD
R CST-KO+Sal
Mp
Cristae
S Cristae surface area
WT+Sal
CST-KO+Sal
WT+CST
CST-KO+CST
Cristae surface area
(% of mito area)
60
40
20
0
*
*
ns
*
SSM
IFM

Fig. 6

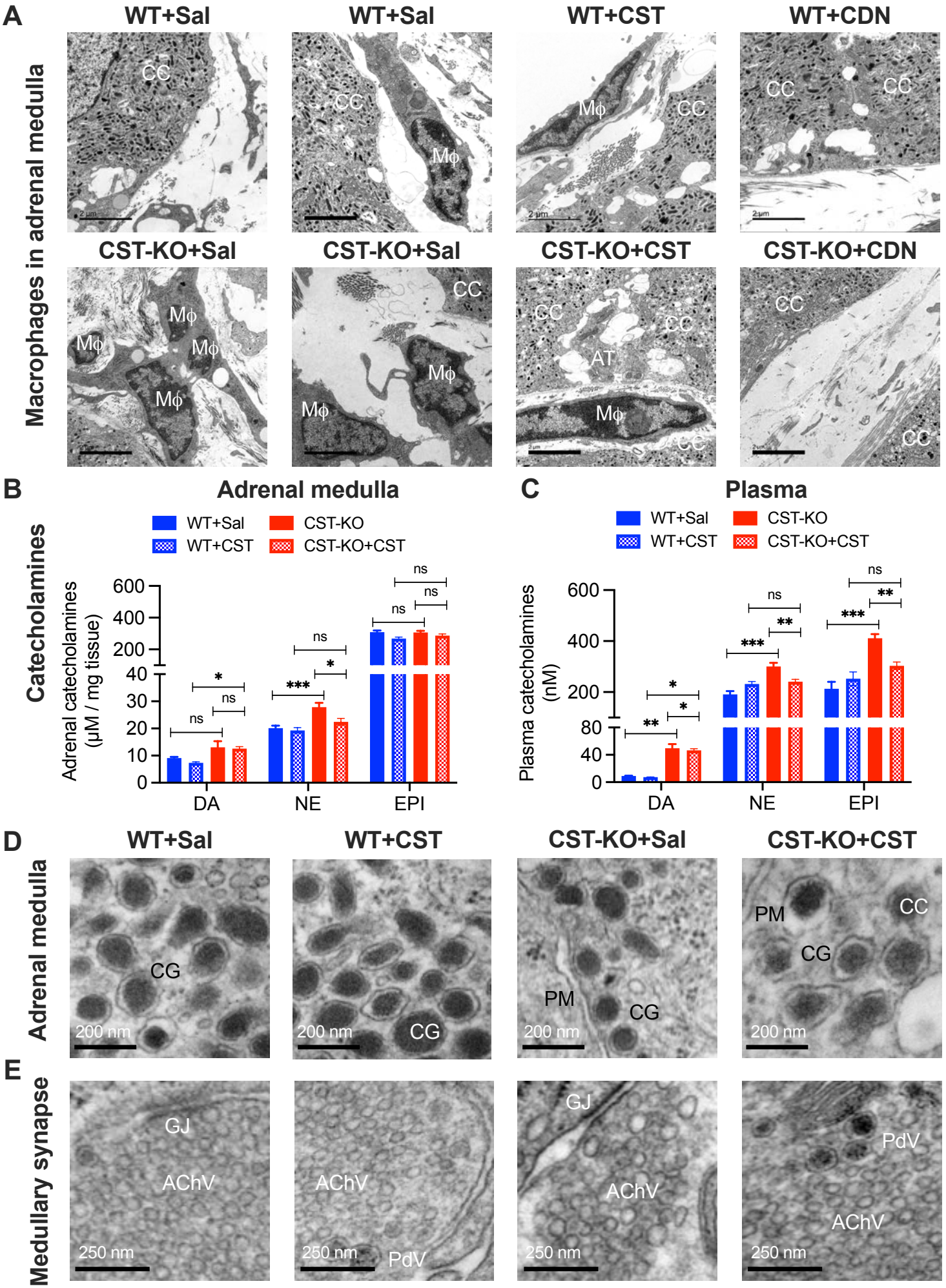
A
WT+Sal
WT+Sal
WT+CST
WT+CDN
Macrophages in adrenal medulla
CC
Mϕ
CST-KO+Sal
CST-KO+Sal
CST-KO+CST
CST-KO+CDN
AT
B
Adrenal medulla
Catecholamines
WT+Sal
WT+CST
CST-KO
CST-KO+CST
Adrenal catecholamines (μM / mg tissue)
600
400
200
40
30
20
10
0
ns
*
***
DA
NE
EPI
C
Plasma
Plasma catecholamines (nM)
80
40
**
D
Adrenal medulla
CG
PM
200 nm
E
Medullary synapse
GJ
AChV
PdV
250 nm

Fig. 7

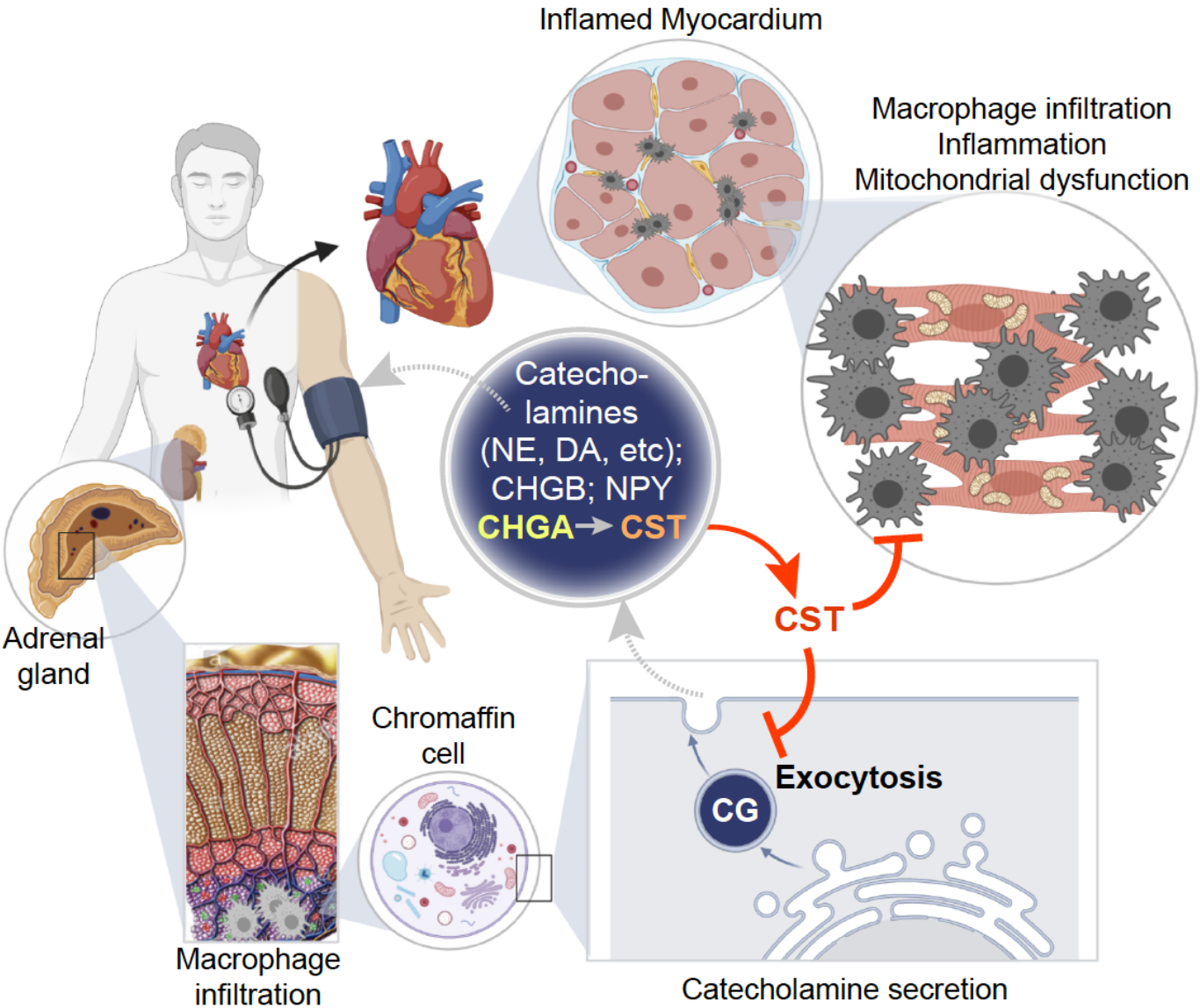
Inflamed Myocardium
Macrophage infiltration
Inflammation
Mitochondrial dysfunction
Catecho-
lamines
(NE, DA, etc);
CHGB; NPY
CHGA→ CST
CST
Adrenal
gland
Chromaffin
cell
Exocytosis
CG
Macrophage
infiltration
Catecholamine secretion

Fig. 8

Supplemental Table S1. Primer sequences used in RT-qPCR experiments

Gene	Gene ID	Forward primer (5'-3')	Reverse primer (3'-5')
Actc1	11464	CTGGATTCTGGCGATGGTGTA	CGGACAATTTCACGTTCAGCA
Ang4	219033	GGTTGTGATTCCTCCAACTCTG	CTGAAGTTTTCTCCATAAGGGCT
Arg1	11846	CTCCAAGCCAAAGTCCTTAGAG	AGGAGCTGTCATTAGGGACATC
Astn2	56079	GCACAGCAGCGGACATTTC	TTCCTCAACGATCTCCGAGGG
Atp5j	11957	TATTGGCCCAGAGTATCAGCA	GGGGTTTGTCGATGACTTCAAAT
Cap1	12331	ATGGCTGACATGCAAAATCTTGT	TGGCAAGCAGCGAGTCAAAT
Ccl2	20296	TTAAAAACCTGGATCGGAACCAA	GCATTAGCTTCAGATTTACGGGT
Cd36	12491	ATGGGCTGTGATCGGAACTG	GTCTTCCCAATAAGCATGTCTCC
Cers2	76893	ATGCTCCAGACCTTGTATGACT	CTGAGGCTTTGGCATAGACAC
Clec10a	17312	TGAGAAAGGCTTTAAGAACTGGG	GACCACCTGTAGTGATGTGGG
Clec7a	56644	GACTTCAGCACTCAAGACATCC	TTGTGTCGCCAAAATGCTAGG
Col1a2	12843	GTAACTTCGTGCCTAGCAACA	CCTTTGTCAGAATACTGAGCAGC
Cxcl1	14825	CTGGGATTCACCTCAAGAACATC	CAGGGTCAAGGCAAGCCTC
Cyb5	109672	GGGCAGTCAGACAAGGATGTG	TCGTACACCTTATGATGCAGGA
Defa20	68009	TGTAGAAAAGGAGGCTGCAATAG	AGAACAAAAGTCGTCCTGAGC
Dgat2	67800	GCGCTACTTCCGAGACTACTT	GGGCCTTATGCCAGGAAACT
Ear11	93726	TGGAGCAACTTGAGTCTCGAC	CGGGGATAGGCTCTGTTATAGA
Emr1	13733	TGACTCACCTTGTGGTCCTAA	CTTCCCAGAATCCAGTCTTTCC
Glo1	109801	GATTTGGTCACATTGGGATTGC	TCCTTTCATTTTCCCGTCATCAG
Gm7120	633640	ACAGAATCCCTCATTTCCAGCA	CCGATCACTCCGTGTACTATGT
Ifng	15978	ATGAACGCTACACACTGCATC	CCATCCTTTTGCCAGTTCCTC
IL10	16153	GCTCTTACTGACTGGCATGA	CGCAGCTCTAGGAGCATGTG
IL12b	16160	TGGTTTGCCATCGTTTTGCTG	ACAGGTGAGGTTCACTGTTTCT
IL4	16189	GGTCTCAACCCCCAGCTAGT	GCCGATGATCTCTCTCAAGTGAT
Itgam	16409	CCATGACCTTCCAAGAGAATGC	ACCGGCTTGTGCTGTAGTC
Itgax	16411	CTGGATAGCCTTTCTTCTGCTG	GCACACTGTGTCCGAACTCA
Mrc1	17533	CTCTGTTCAGCTATTGGACGC	CGGAATTTCTGGGATTCAGCTTC
Myl4	17896	AAGAAACCCGAGCCTAAGAAGG	TGGGTCAAAGGCAGAGTCCT
Myl7	17898	GGCACAACGTGGCTCTTCTAA	TGCAGATGATCCCATCCCTGT
Ndufa3	66091	ATGGCCGGGAGAATCTCTG	AGGGGCTAATCATGGGCATAAT
Nos2	18126	GTTCTCAGCCCAACAATACAAGA	GTGGACGGGTCGATGTCAC
Nppa	230899	GCTTCCAGGCCATATTGGAG	GGGGGCATGACCTCATCTT
Pam	18484	CTGGGGTCACACCTAAAGAGT	ATGAGGGCATGTTGCATCCAA
Pdk2	18604	AGGGGCACCCAAGTACATC	TGCCGGAGGAAAGTGAATGAC
Pfkm	18642	TGTGGTCCGAGTTGGTATCTT	GCACTTCCAATCACTGTGCC
Ppara	19013	AGAGCCCCATCTGTCCTCTC	ACTGGTAGTCTGCAAAACCAAA
Sdhc	66052	GCTGCGTTCTTGCTGAGACA	ATCTCCTCCTTAGCTGTGGTT

Slc27a1	26457	CGCTTTCTGCGTATCGTCTG	GATGCACGGGATCGTGTCT
Slc27a2	26458	TCCTCCAAGATGTGCGGTACT	TAGGTGAGCGTCTCGTCTCG
Slc2a4	20528	GTGACTGGAACACTGGTCCTA	CCAGCCACGTTGCATTGTAG
Sptlc1	268656	ACGAGGCTCCAGCATACCAT	TCAGAACGCTCCTGCAACTTG
Tnf	21926	CCCTCACACTCAGATCATCTTCT	GCTACGACGTGGGCTACAG
Tnni3	21954	TCTGCCAACTACCGAGCCTAT	CTCTTCTGCCTCTCGTTCCAT
Tnnt2	21956	CAGAGGAGGCCAACGTAGAAG	CTCCATCGGGGATCTTGGGT
Tpm1	22003	CAGAAGGCAAATGTGCCGAG	TCCAGCATCTGGTGCATACTA
Ttn	22138	GACACCACAAGGTGCAAAGTC	CCCACTGTTCTTGACCGTATCT

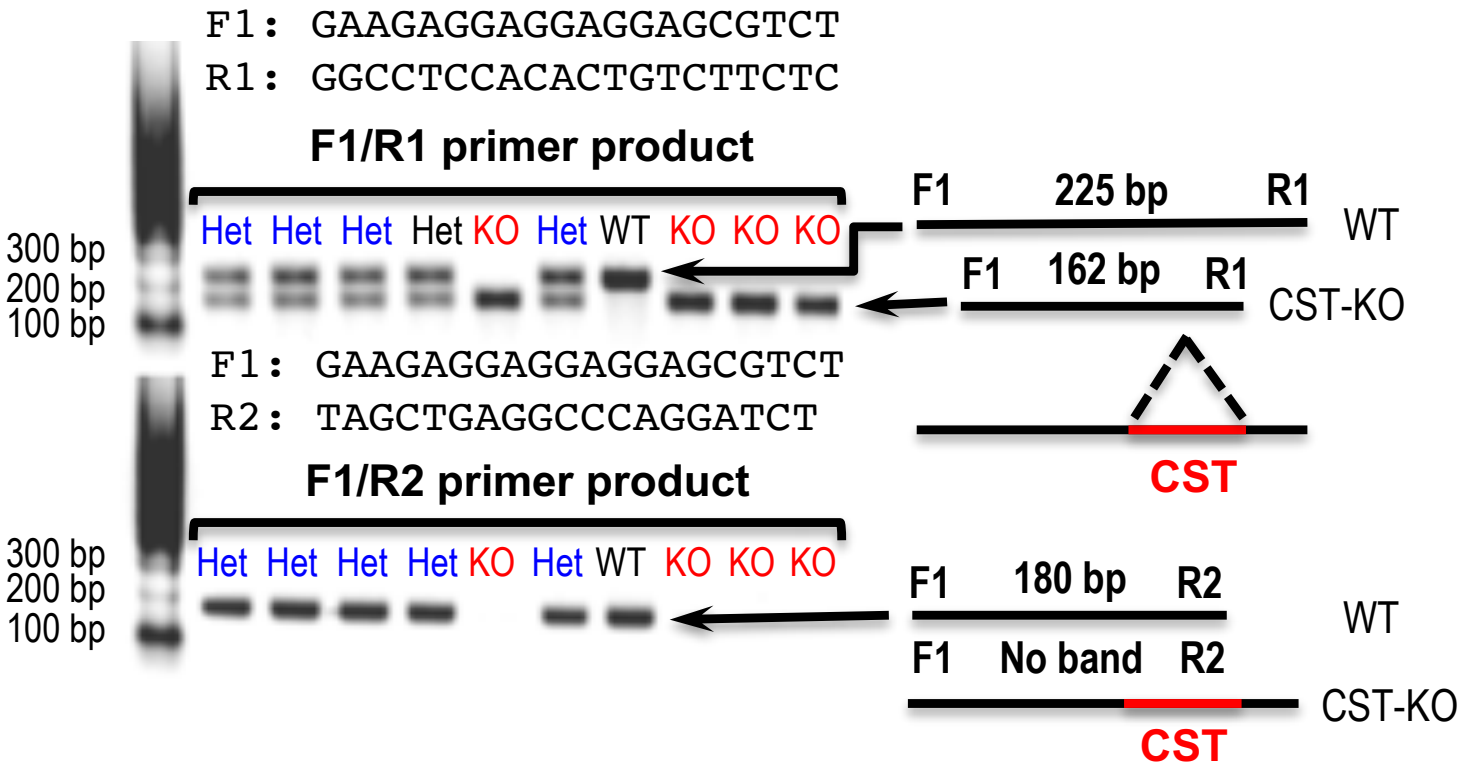
F1: GAAGAGGAGGAGGAGCGTCT
R1: GGCCTCCACACTGTCTTCTC
F1/R1 primer product
Het Het Het Het KO Het WT KO KO KO
300 bp
200 bp
100 bp
F1 225 bp R1
WT
F1 162 bp R1
CST-KO
F1: GAAGAGGAGGAGGAGCGTCT
R2: TAGCTGAGGCCCAGGATCT
CST
F1/R2 primer product
Het Het Het Het KO Het WT KO KO KO
300 bp
200 bp
100 bp
F1 180 bp R2
WT
F1 No band R2
CST-KO
CST

Fig. S1

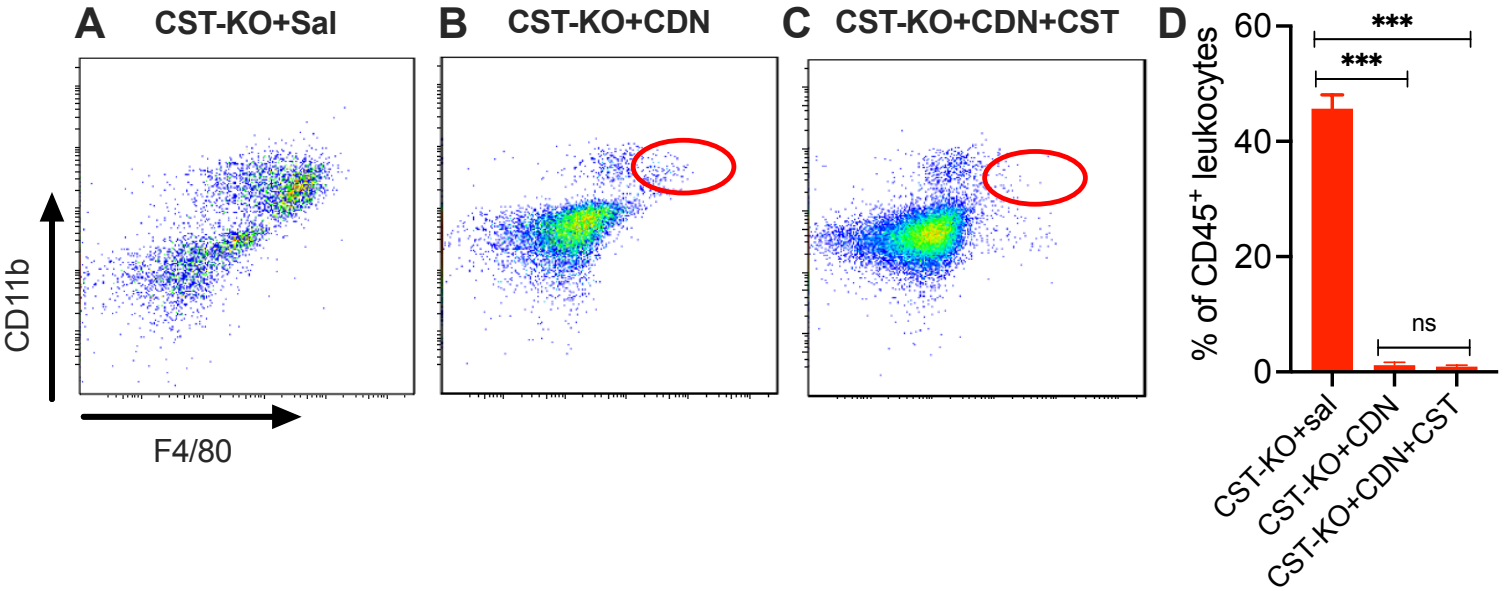
A
CST-KO+Sal
B
CST-KO+CDN
C
CST-KO+CDN+CST
D
CD11b
F4/80
% of CD45+ leukocytes
60
40
20
0
***
***
ns
CST-KO+sal
CST-KO+CDN
CST-KO+CDN+CST

Fig. S2

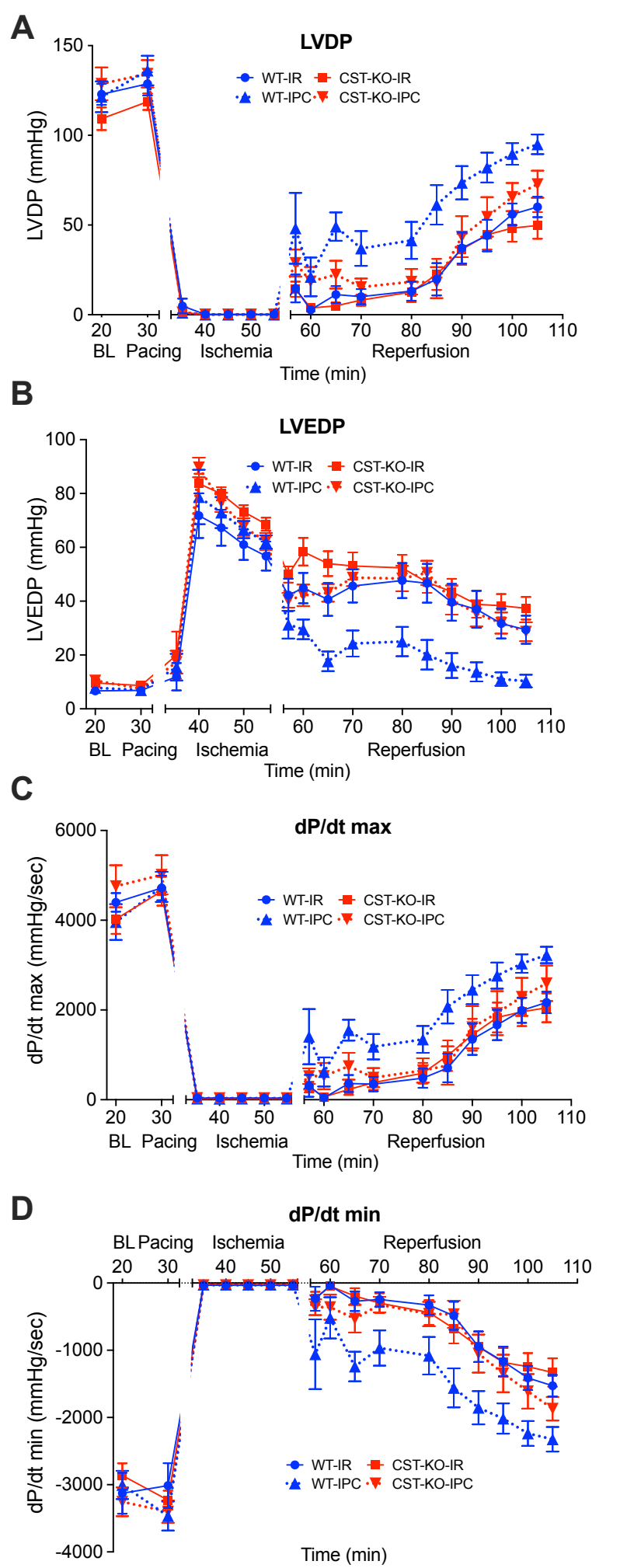
A
LVDP
WT-IR
CST-KO-IR
WT-IPC
CST-KO-IPC
LVDP (mmHg)
150
100
50
0
20
30
40
50
60
70
80
90
100
110
BL
Pacing
Ischemia
Reperfusion
Time (min)
B
LVEDP
LVEDP (mmHg)
100
80
60
40
20
0
C
dP/dt max
dP/dt max (mmHg/sec)
6000
4000
2000
0
D
dP/dt min
dP/dt min (mmHg/sec)
0
-1000
-2000
-3000
-4000

Fig. S3